Physics processes in hadronic showers

Calor2000

Annecy, 9-14 October 2000

A. Ferrari, P.R. Sala

CERN, Geneva Switzerland (on leave from INFN-Milan)

Topics

- A few words about Hadron-Nucleus (h-A) interactions and their modelling
- Features of h-A of relevance for calorimetry
- The π^0 and γ production and e/h
- Binding energy and energy conservation
- The role of slow neutron interactions
- Slow charged fragments and signal quenching
- A few real life examples

Main steps of h-A interactions

High-energy h-A interactions can be schematically described as a sequence of the following steps:

- *Glauber-Gribov cascade and high energy collisions*
- *(Generalized)-IntraNuclear cascade*
- *Preequilibrium emission*
- *Evaporation/Fragmentation/Fission and final deexcitation*

The following aspects are of direct relevance for calorimetry:

- *Multiplicity distribution of fast (relativistic) particles*
- π^0 *and* γ *production and its scaling with projectile energy*
- *Slow fragment and neutron production: the asymptotic regime of the target fragmentation part of the collision*
- *Binding energy losses*

h-A interactions

The approach to hadronic interaction modelling presented in the following is the one adopted by most state-of-the-art codes

In this "microscopic" approach, each step has sound physical basis. The performances are optimized comparing with particle production data at single interaction level. No tuning whatsoever on "integral" data, like calorimeter resolutions, thick target yields etc, is performed

The final predictions are obtained with minimal free parameters, fixed for all energies and target/projectile combinations

Results in complex cases as well as scaling laws and properties come out naturally from the underlying physical models. The basic conservation laws are fulfilled "a priori"

All the examples/results presented in the following have been obtained with FLUKA *and should be typical of codes adopting similar approaches*

Hadron-nucleon interaction models

Elastic, charge exchange and strangeness exchange reactions:

- Available phase-shift analysis and/or fits of experimental differential data
- At high energies, standard eikonal approximations are used

Particle production interactions: two kind of models

- Those based on "resonance" production and decays, which cover the energy range up to 3–5 GeV
- Those based on quark/parton string models, which provide reliable results up to several tens of TeV

Nonelastic hN interactions at intermediate energies

- $N_1 + N_2 \rightarrow N_1' + N_2' + \pi$ threshold around 290 MeV, important above 700 MeV,
- $\pi + N \rightarrow \pi' + \pi'' + N'$ opens at 170 MeV.

Dominance of the Δ resonance and of the N^* resonances $\rightarrow$ reactions treated in the framework of the isobar model $\rightarrow$ all reactions proceed through an intermediate state containing at least one resonance.

$$
\begin{aligned}
N_1 + N_2 &\rightarrow N_1' + \Delta(1232) \rightarrow N_1' + N_2' + \pi \\
\pi + N &\rightarrow \Delta(1600) \rightarrow \pi' + \Delta(1232) \rightarrow \pi' + \pi'' + N' \\
N_1 + N_2 &\rightarrow \Delta_1(1232) + \Delta_2(1232) \rightarrow N_1' + \pi_1 + N_2' + \pi_2
\end{aligned}
$$

Resonance energies, widths, cross sections, branching ratios from data and conservation laws, whenever possible. Inferred from inclusive cross sections when needed

Inelastic hN at high energies: (DPM, QGSM, ...)

- Problem: "soft" interactions $\rightarrow$ no perturbation theory.
- Solution : Interacting strings (quarks held together by the gluon-gluon interaction into the form of a string)
- Interactions treated in the Reggeon-Pomeron framework
- At sufficiently high energies the leading term corresponds to a Pomeron (IP) exchange (a closed string exchange)
- Each colliding hadron splits into two colored partons $\rightarrow$ combination into two color neutral chains $\rightarrow$ two back-to-back jets
- Physical particle exchange produce single chains at low energies
- Higher order contributions with multi-Pomeron exchanges important at $E_{lab} \geq$ 1 TeV

DPM and hadronization

from DPM:

- Number of chains
- Chain composition
- Chain energies and momenta
- Diffractive events

Almost No Freedom

Chain hadronization

- Assumes chain universality
- Fragmentation functions from hard processes and e^+e^-
- Transverse momentum from uncertainty considerations
- Mass effects at low energies

The same functions and (few) parameters for all reactions and energies

DPM: chain examples

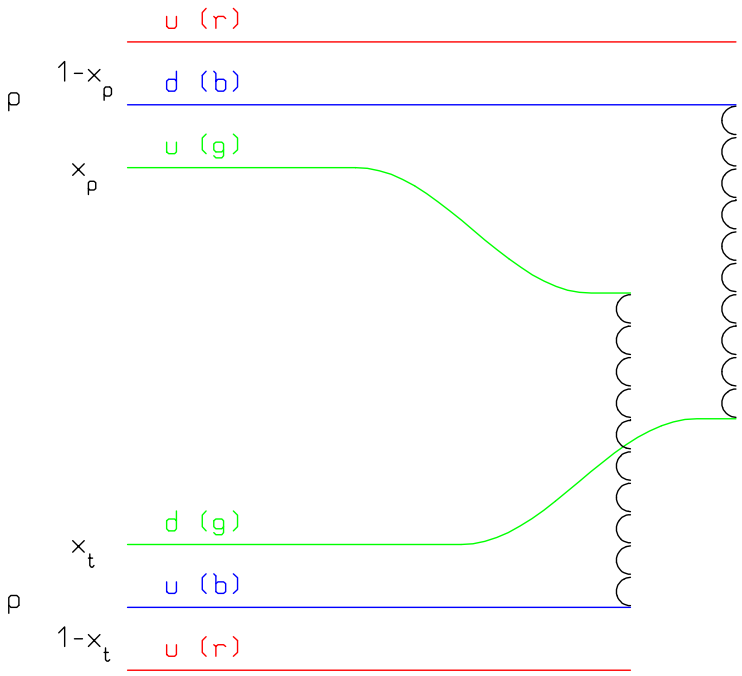

Leading two-chain diagram in DPM for $p-p$ scattering. The color (red, blue, and green) and quark combination shown in the figure is just one of the allowed possibilities

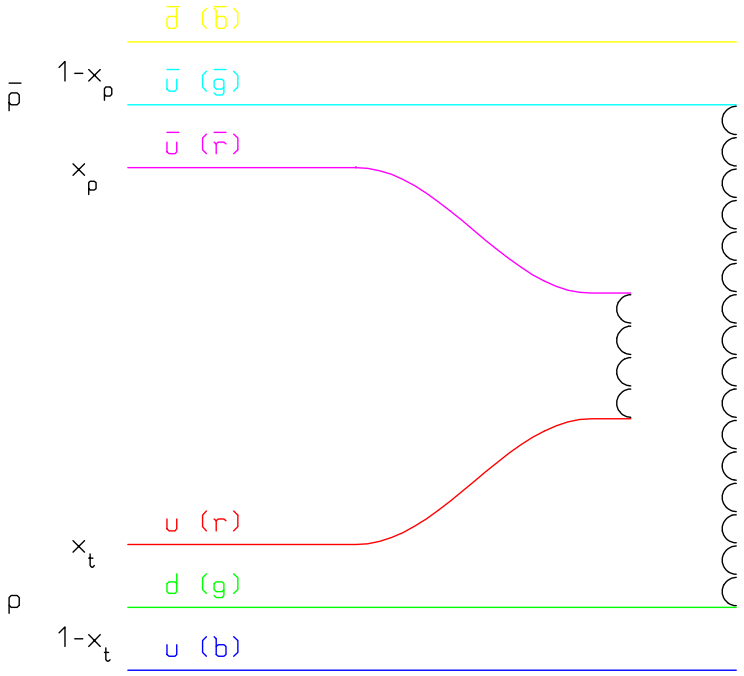

Leading two-chain diagram in DPM for $\bar{p}-p$ scattering. The color (red, blue, and green) and quark combination shown in the figure is just one of the allowed possibilities

DPM: chain examples II

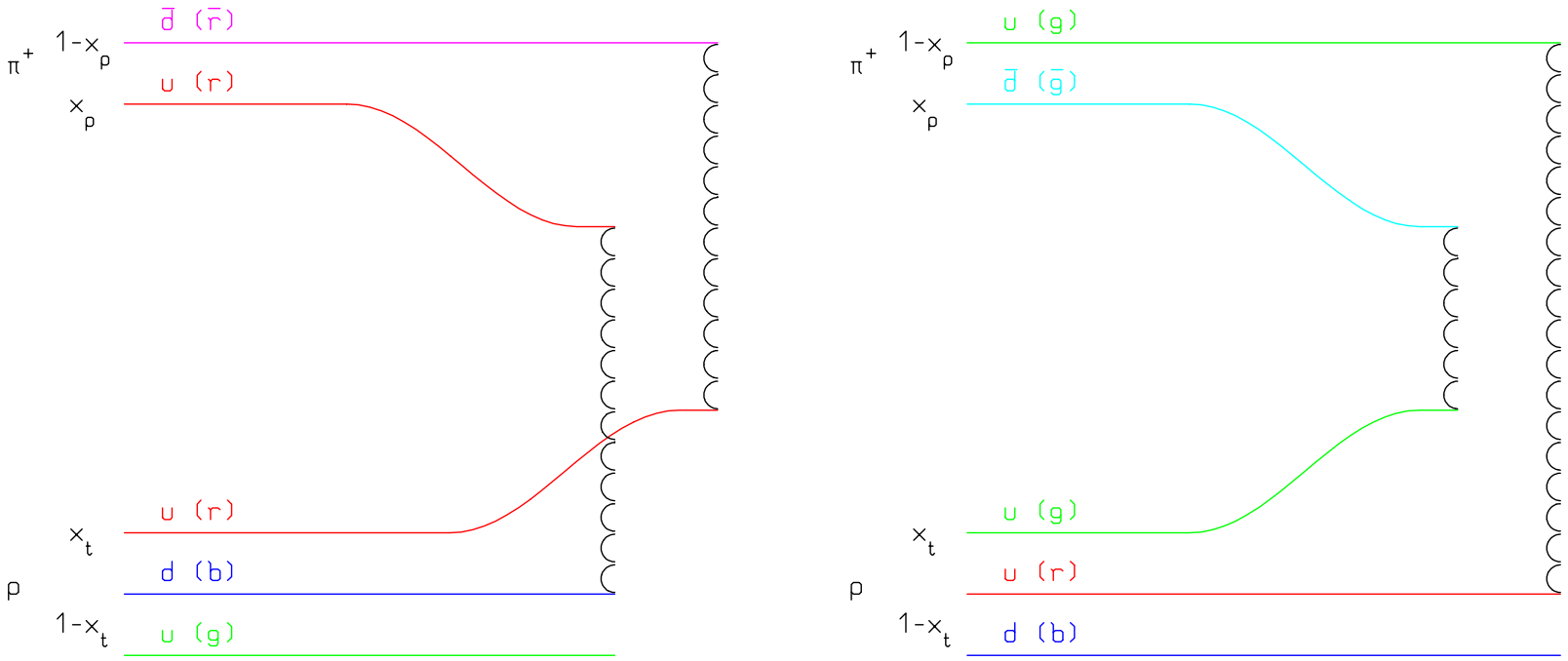

Leading two-chain diagrams in DPM for $\pi^+ - p$ scattering. The color (red, blue, and green) and quark combination shown in each figure is just one of the allowed possibilities

Nonelastic hN at high E :(π^+ p), 7-22 GeV

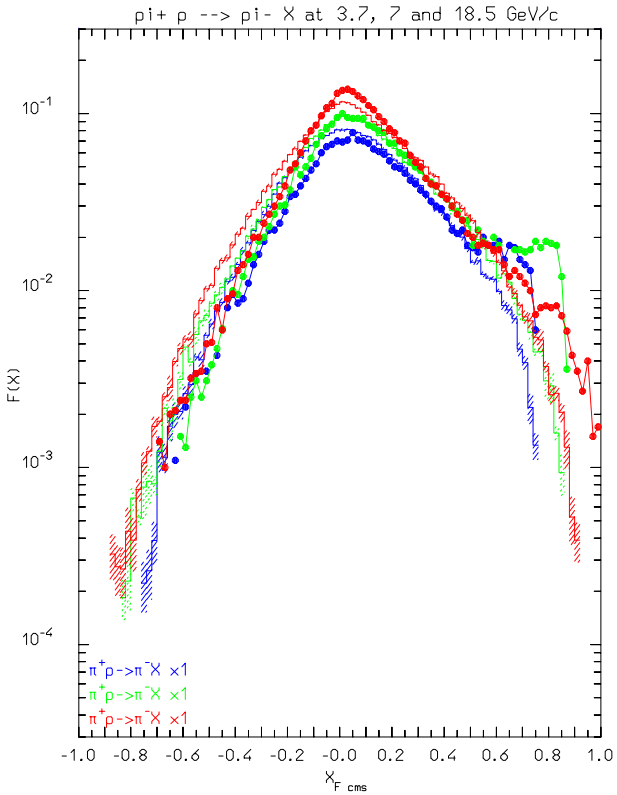

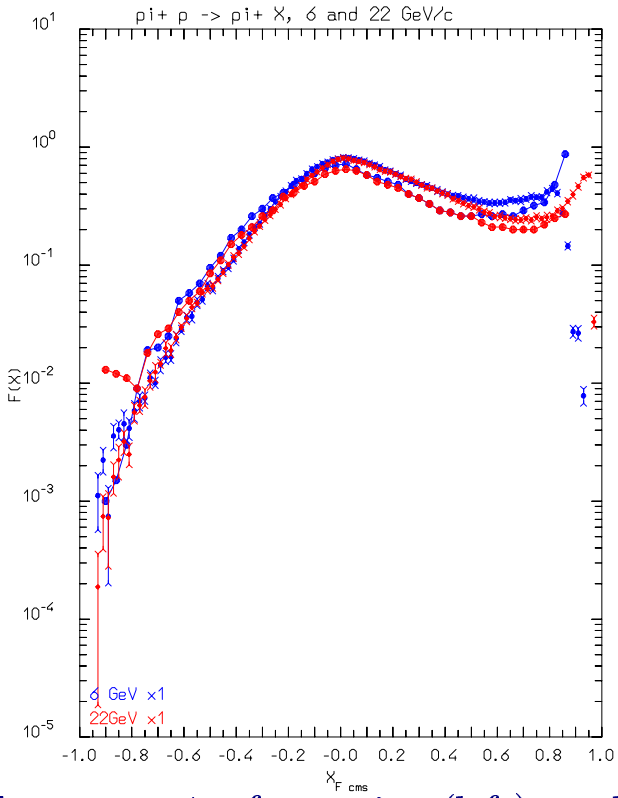

Invariant cross section spectra, as a function of Feynman x_F^* of negative (left), and positive (right) pions emitted for π^+ on protons at various momenta. Data from M.E Law et al. LBL80 (1972).

Nonelastic hN high E: (K^-p) , (π^-p) 10-16 GeV, p_T

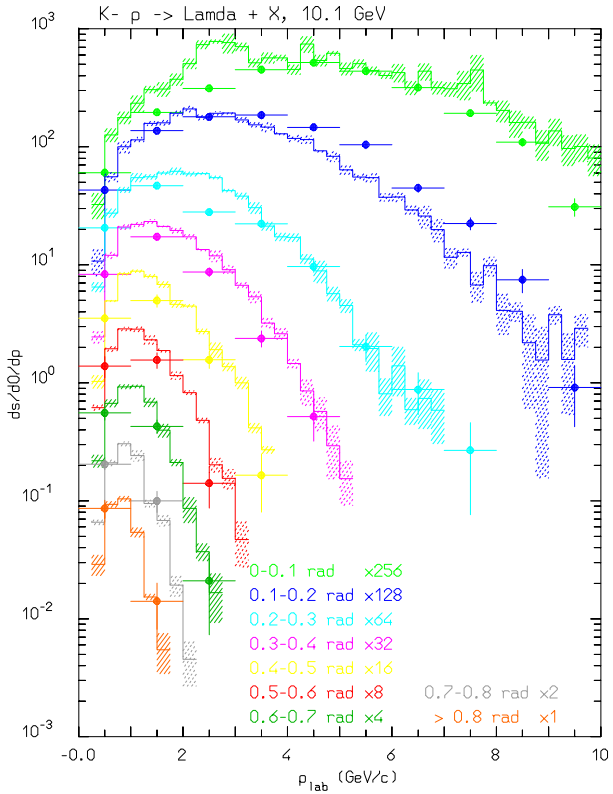

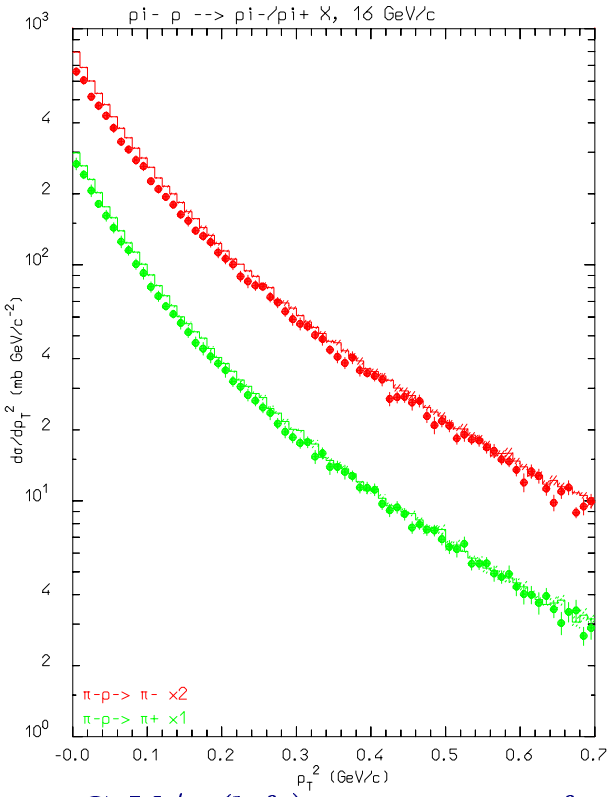

Double differential cross section for $K^-p \to \Lambda X$ at 10 GeV/c (left), p_T spectra of π^+ and π^- produced by 16 GeV/c π^- incident on an hydrogen target. Data from M.E Law et al. LBL80 (1972).

Nonelastic hN high E: (π^+ p) 250GeV, x_F and p_t

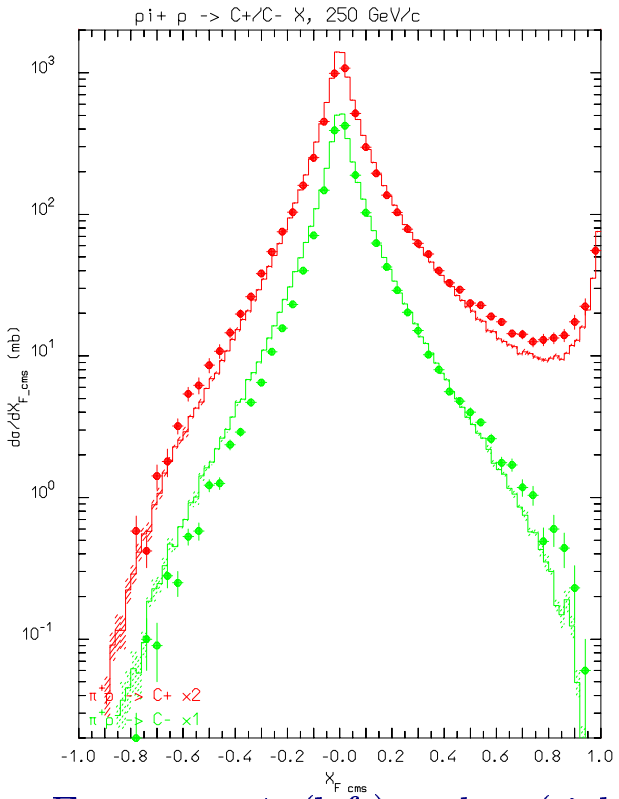

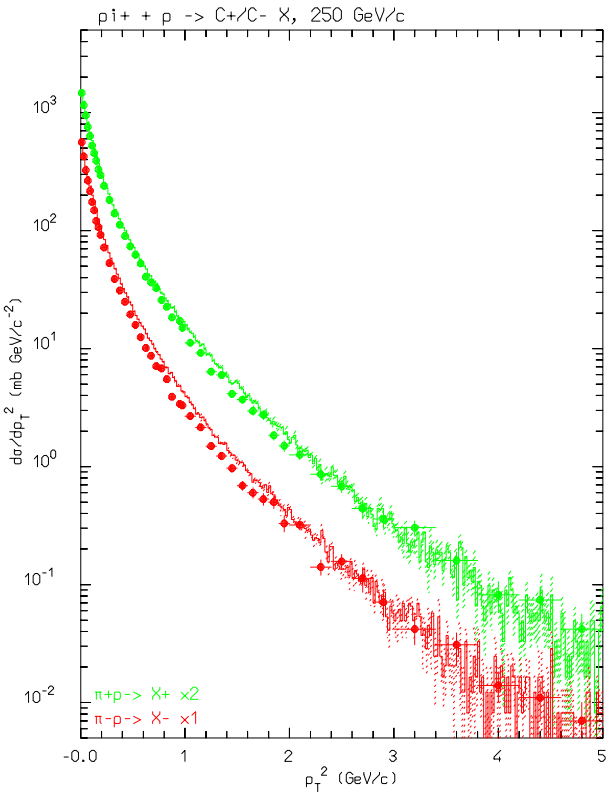

Feynman x_F^* (left) and p_t (right) spectra of positive particles and π^- produced by 250 GeV/c π^+ incident on an hydrogen target. Exp. data (symbols) have been taken from M. Adamus et al. ZPC39, 311 (1988).

(Generalized) IntraNuclear Cascade basic assumptions

1. Primary and secondary particles moving in the nuclear medium
2. Interaction probability from σ_{free} + Fermi motion $\times$ $\rho(r)$ + exceptions (ex. π)
3. *Glauber cascade at high energies*
4. Classical trajectories $(+)$ nuclear mean potential (*resonant for π's!!*)
5. Curvature from nuclear potential $\rightarrow$ refraction and reflection.
6. Interactions are incoherent and uncorrelated
7. Interactions in projectile–target nucleon CMS $\rightarrow$ Lorentz boosts
8. *Multibody absorption for π, μ^-, K^-*
9. *Quantum effects (Pauli, formation zone, correlations...)*
10. *Exact conservation of energy, momenta and all additive quantum numbers,including nuclear recoil*

h-A at high energies: the Glauber Cascade

Elastic, Quasi-elastic and Absorption hA cross sections derived from Free hadron-Nucleon cross section + Nuclear ground state ONLY.

Inelastic interaction $\equiv$ multiple interaction with ν target nucleons, with binomial distribution (at a given impact parameter, b):

$$P_{r\ \nu}(b) \equiv \begin{pmatrix} A \\ \nu \end{pmatrix} P_r^{\nu}(b) \left[1 - P_r(b)\right]^{A-\nu}$$

where $P_r(b) \equiv \sigma_{hN\ r} T_r(b)$, and $T_r(b)$= profile function *(folding of nuclear density and scattering profiles along the path).*

On average :

$$< \nu > \ = \ \frac{Z\sigma_{hp\ r} + N\sigma_{hn\ r}}{\sigma_{hA\ abs}}$$

$$\sigma_{hA\ abs}(s) \ = \ \int \mathrm{d}^2\vec{b} \left[1 - \left(1 - \sigma_{hN\ r}(s) T_r(b)\right)^A\right]$$

h-A at high energies: Glauber-Gribov

Glauber-Gribov = diagram interpretation of the Glauber cascade

Used by QGSM/DPM/... for modelling Multiple Collisions

Interaction with ν target nucleons

$\Downarrow$

2ν chains, out of which

2 chains struck between the projectile and target valence (di)quarks,

$2(\nu - 1)$ chains between projectile sea $q - \bar{q}$ and target valence (di)quarks.

No freedom, except in the treatment of mass effects at low energies.

Fermi motion included $\rightarrow$ smearing of p_T distributions

(G)INC follows

Nonelastic hA interactions at high energies: examples

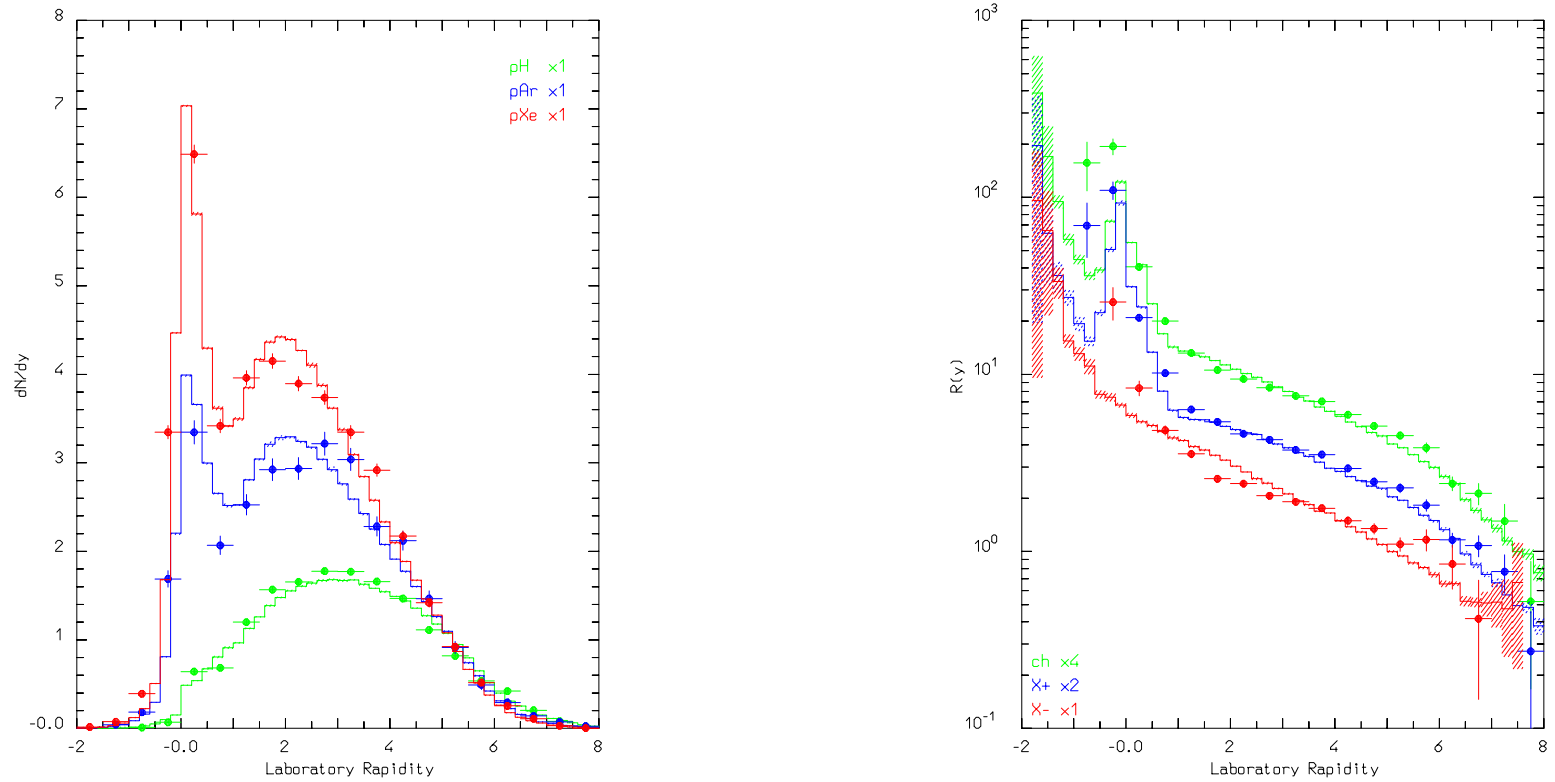

Rapidity distribution of charged particles produced in 200 GeV proton collisions on Hydrogen, Argon, and Xenon target (left) and ratio of rapidity distribution of charged, positive, and negative particles produced in 200 GeV proton collisions on Xenon and Hydrogen (right). Data from C. De Marzo et al., PRD26, 1019 (1982).

Nonelastic hA interactions at high energies: examples

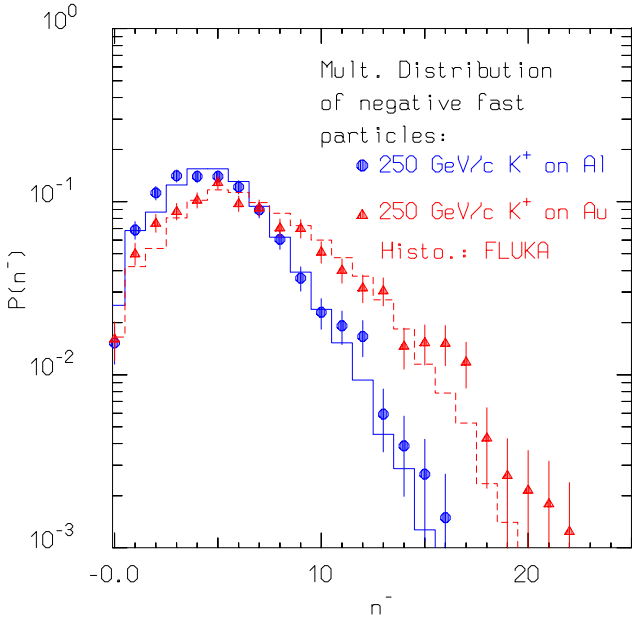

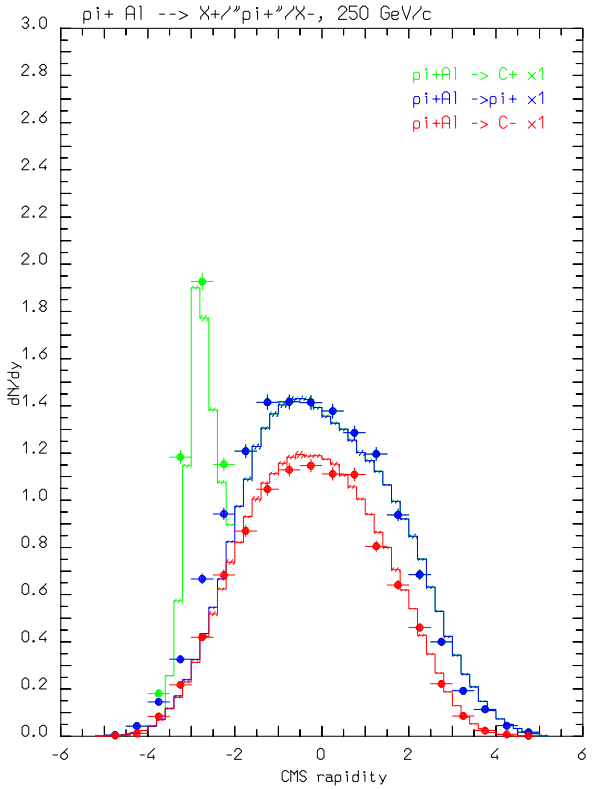

Multiplicity distribution of negative shower particles for 250 GeV/c K^+ on Aluminium and Gold targets (left), and rapidity distribution of positive, negative, and "π^+" particle for 250 GeV/c π^+ on Aluminium (right). Data from I.V. Ajinenko et al. ZPC42 377 (1989) and N.M. Agababyan et al. ZPC50 361 (1991).

h-A interactions: the multiplicity distribution vs the Glauber cascade

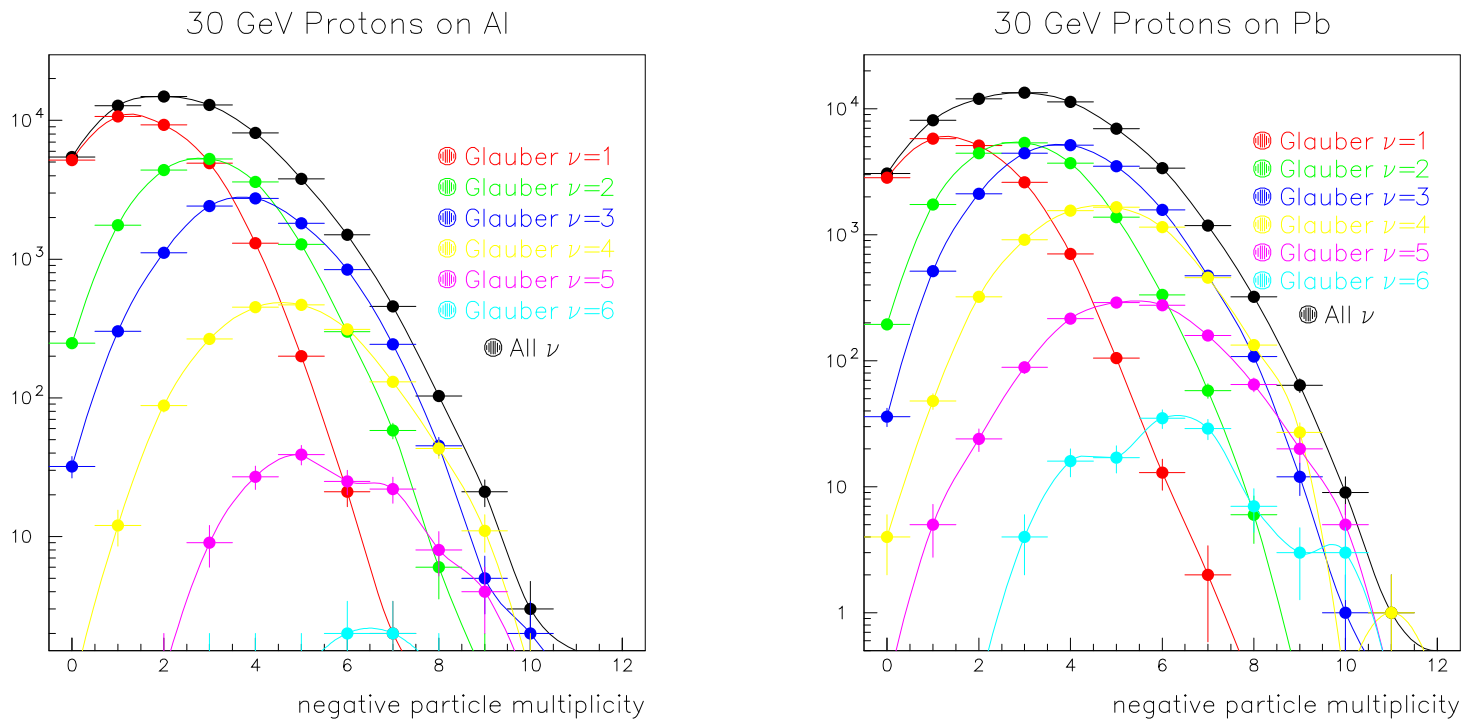

Negative particle multiplicity distribution for 30 GeV protons on Al (left) and Pb (right), total and for given numbers of primary collisions

Quantistic effects in (G)INC

1. Pauli blocking,
2. *Formation time (inelastic),*
3. Coherence length ((quasi)-elastic and charge exchange),
4. Nucleon antisymmetrization,
5. Hard core nucleon correlations

Formation Zone

Naively: "materialization" time. Qualitative estimate: in the frame where $p_{\|} = 0$

$$\bar{t} \;=\; \Delta t \approx \frac{\hbar}{E_T} = \frac{\hbar}{\sqrt{p_T^2 + M^2}}$$

particle proper time

$$\tau \;=\; \frac{M}{E_T}\bar{t} = \frac{\hbar M}{p_T^2 + M^2}$$

Going to lab system

$$t_{lab} \;=\; \frac{E_{lab}}{E_T}\bar{t} = \frac{E_{lab}}{M}\tau = \frac{\hbar E_{lab}}{p_T^2 + M^2}$$

As a function of particle rapidity y

$$t_{lab} = \bar{t}\cosh y = \frac{\hbar}{\sqrt{p_T^2 + M^2}}\cosh y$$

Condition for possible reinteraction inside a nucleus:

$$v \cdot t_{lab} \leq R_A \approx r_0 A^{\frac{1}{3}}$$

Comparison with SPY I

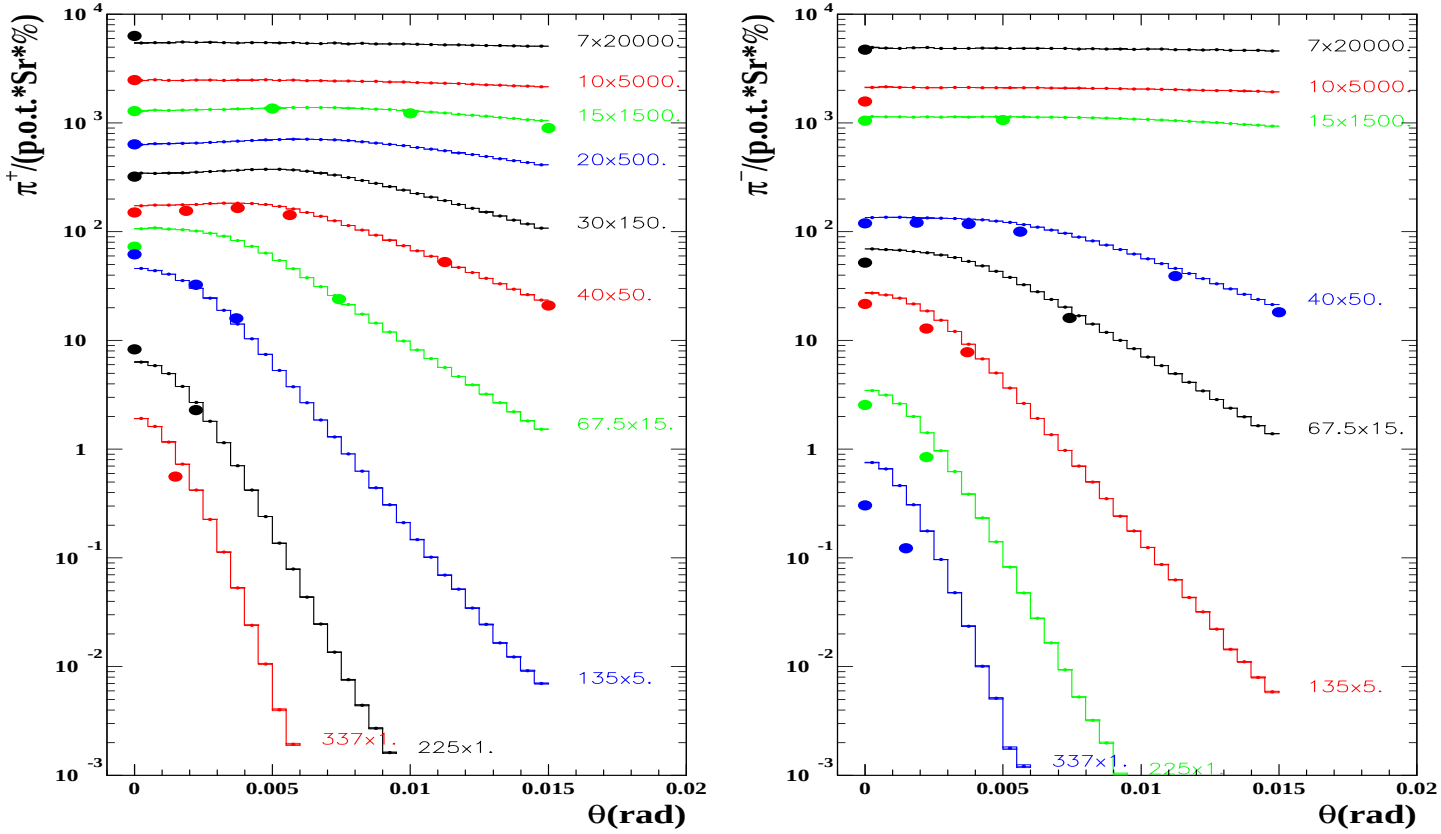

Double differential cross section for π^+ (left) and π^- (right) production for 450 GeV/c protons on a 10 cm thick Be target (data from H.W. Atherton CERN 80–07, G. Ambrosini et al. PL B425 208 (1998)).

Comparison with SPY II

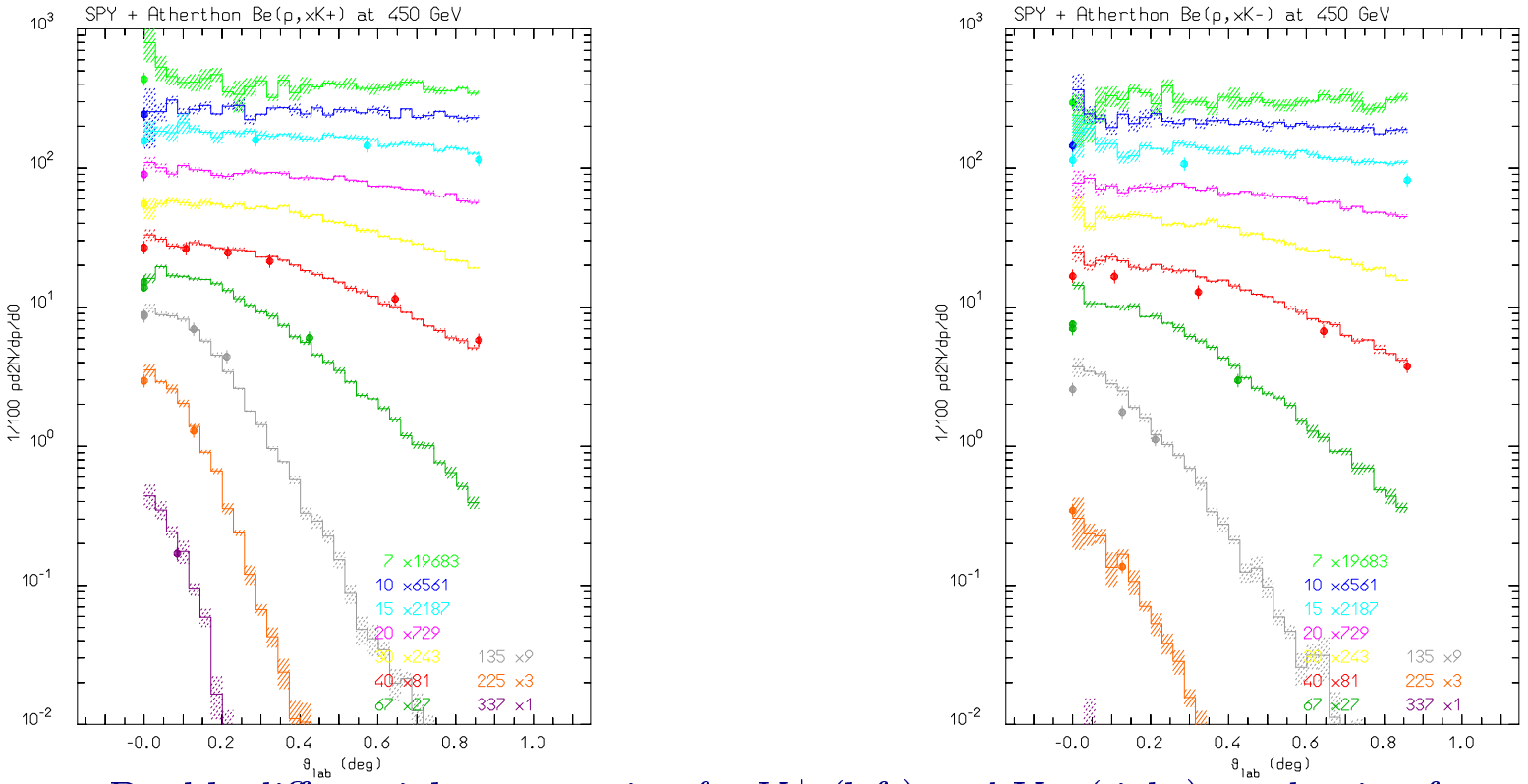

Double differential cross section for K^+ (left) and K^- (right) production for 450 GeV/c protons on a 10 cm thick Be target (data from H.W. Atherton CERN 80–07, G. Ambrosini et al. PL B425 208 (1998)).

Nonelastic hA at high E: (p,Be), 14-24 GeV

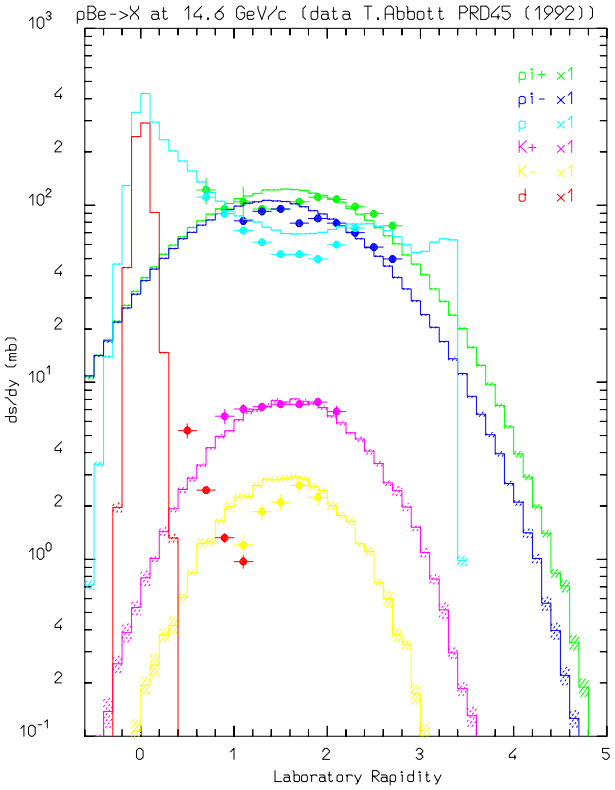

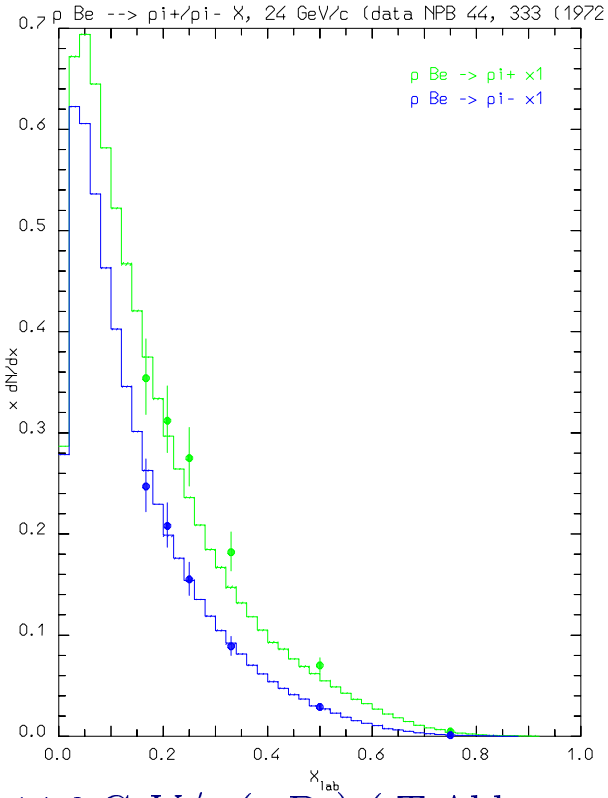

Left: rapidity distribution of $\pi^{+/-}$, $K^{+/-}$, p and d, 14.6 GeV/c (p,Be) (T.Abbott et al PRD45(11), 3906 (1992)). Right: X_{lab} distribution for $\pi^{+/-}$, 24 GeV/c (p,Be) (symbols extrapolated from the DDCS in T.Eichten et al. NPB 44, 333 (1972)).

Preequilibrium

For E $>$ π production threshold $\rightarrow$ only (G)INC models

At lower energies$\rightarrow$ a variety of preequilibrium models

Two leading approaches

the quantum-mechanical multistep model	the exciton model
Very good theoretical background	statistical assumptions
complex, difficulties for multiple emission	simple and fast

Exciton model: chain of steps, each (n_{th}) step corresponding to N_n

"excitons" == either a particle above or a hole below the Fermi surface

Statistical assumption: any partition of the excitation energy E among N, $N = N_h + N_p$, excitons has the same probability to occur

Step: nucleon-nucleon collision with $N_{n+1} = N_n + 2$ ("never come back" approximation)

Chain end = equilibrium = N_n sufficiently high or excitation energy below threshold

N_1 depends on the reaction type and on the cascade history

Evaporation, fission and nuclear break-up

The evaporation probability for a particle of type j , mass m_j, spin $S_j \cdot \hbar$ and kinetic energy E and the total fission probability are given by

$$P_j = \frac{(2S_j+1)m_j}{\pi^2\hbar^3}\int_{V_j}^{U_i-Q_j-\Delta_f}\sigma_{\text{inv}}\frac{\rho_f(U_f)}{\rho_i(U_i)}EdE$$

$$P_F = \frac{1}{2\pi\hbar}\frac{1}{\rho_i(U_i)}\int_0^{(U-B_F)}\rho_F(U-B_F-E)dE$$

- ρ's: nuclear level densities ($\rho_f(U_f)$ for the final nucleus, $\rho_i(U_i)$ for the initial one, $\rho_F(U_F)$ for the fissioning nucleus at the saddle point),
- $U_i \equiv U$: excitation energy of the evaporating nucleus,
- $U_f = U - E - Q_j$: that of the final one,
- $U_F = U - B_F$: excitation energy of the fissioning nucleus at the saddle point (B_F is the fission barrier)
- Q_j: reaction Q for emitting a particle of type j,
- V_j: (possible) Coulomb barrier for emitting a particle of type j,
- σ_{inv}: cross section for the inverse process.

Evaporation, fission and nuclear break-up cont.d

The level density can be assumed to be:

$$\rho(U)dU = \frac{e^{2\sqrt{a(U-\Delta)}}}{12\sqrt{\pi}a^{\frac{1}{4}}(U-\Delta)^{\frac{5}{4}}}dU$$

$$P_j(E)dE \approx K\ Ee^{-\frac{E}{T}}dE$$

- a: level density parameter ($\approx A/8$ MeV^{-1})
- Δ: pairing energy
- T: nuclear temperature (MeV), ($T \approx \sqrt{(U-\Delta)/a}$)

- *Neutrons emission is favoured for medium-heavy nuclei*
- *For the same excitation, the neutron multiplicity is larger for heavier nuclei*
- *The excitation is higher for heavier nuclei due to the larger cascading chances*

h-A interactions: the electromagnetic component

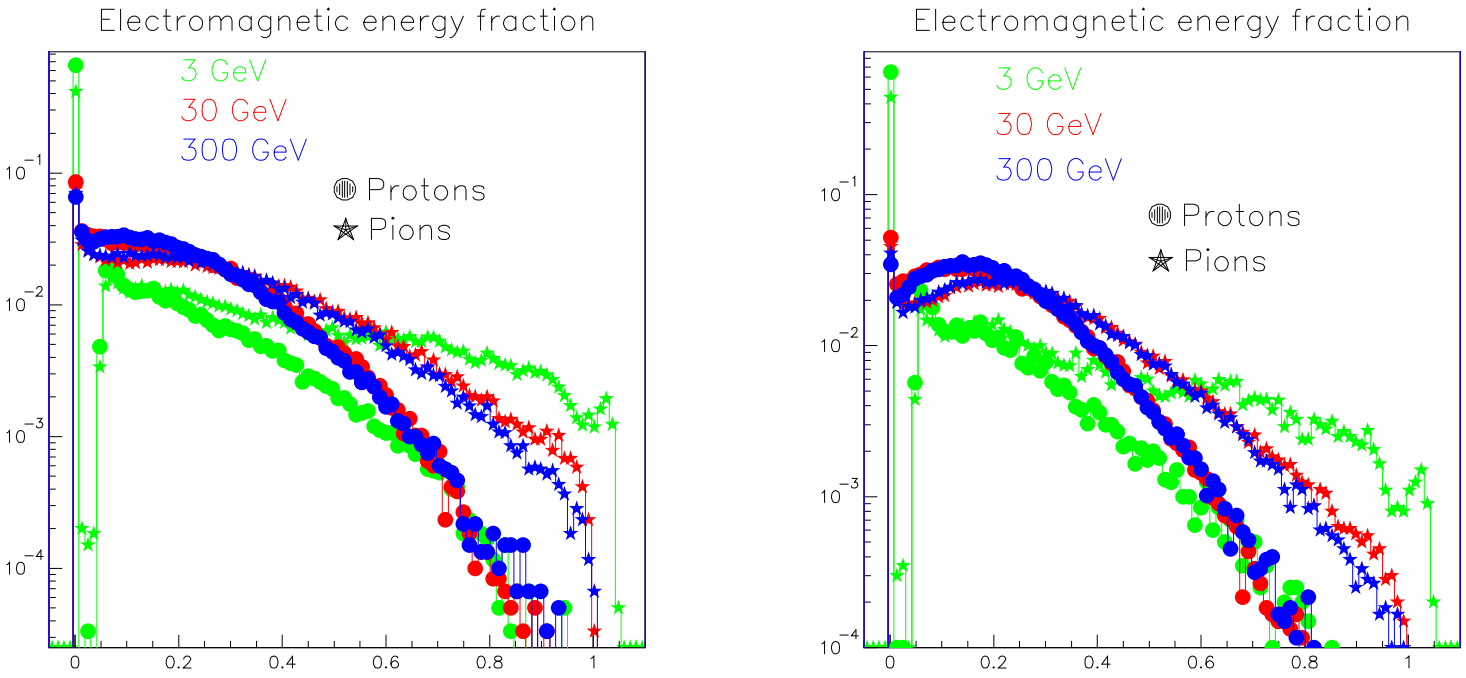

Distribution of the energy fraction carried by π^0's and γ's for interactions in aluminium (left) and lead (right)

h-A interactions: the scaling of the electromagnetic component

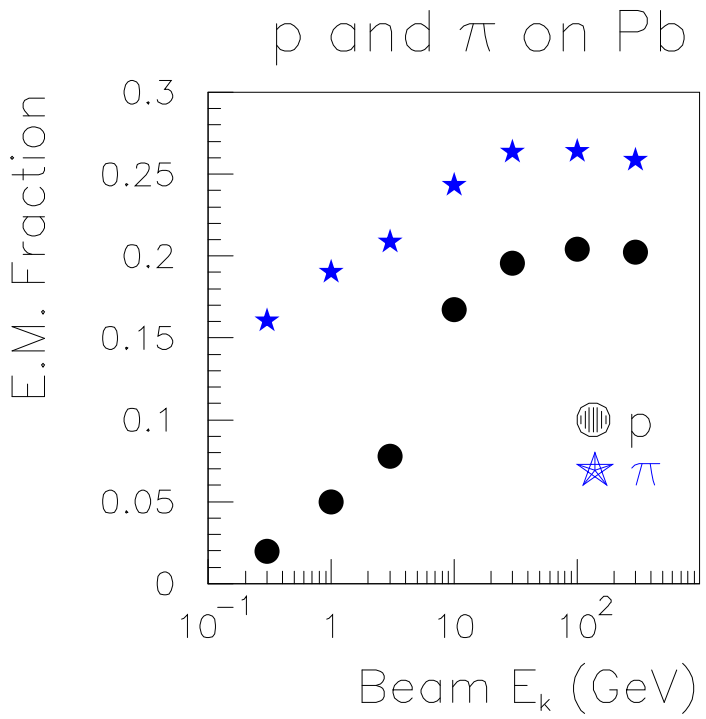

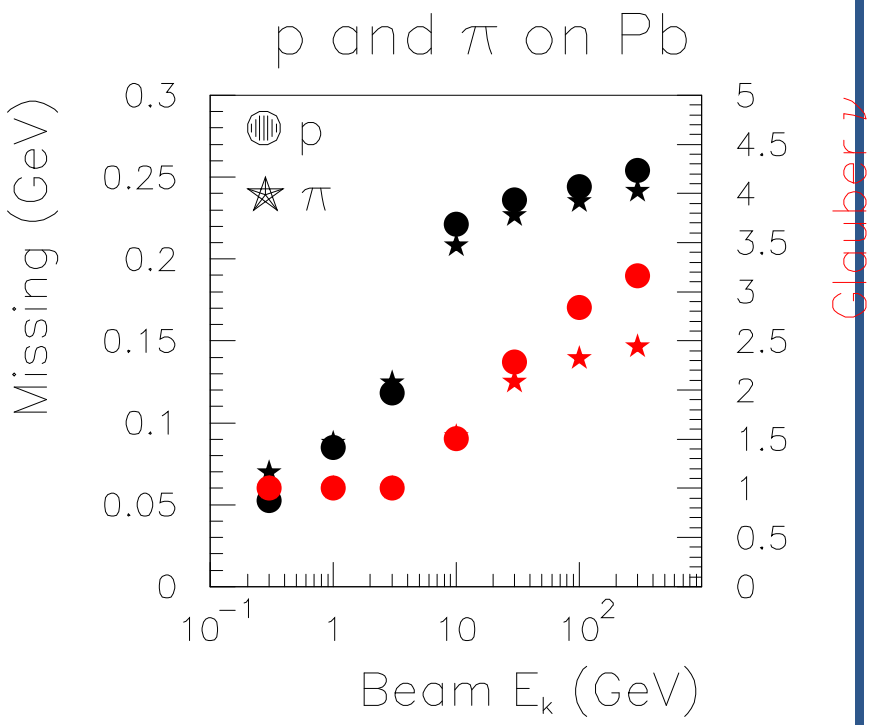

Average energy fraction carried by π^0's and γ's (left) and binding energy losses (right) for interactions in lead. The number of primary collisions are also reported in the last plot

h-A at high energies: the invariance of the target fragmentation region

The Glauber cascade and the formation zone act together in reaching a regime where the "slow" part of the interaction is almost independent of the particle energy

This regime can be easily verified looking at charged particle average multiplicities and multiplicity distributions as a function of energy

- "Fast" tracks, coming from the projectile primary interactions, show the typical $\approx$ logarithmic increase observed for hN interactions
- "Gray" tracks, mostly due to intranuclear cascade reinteractions tend to saturate just above 10 GeV
- "Black" tracks, mostly due to evaporation charged particles saturate as well

Nonelastic hA interactions at high energies: examples

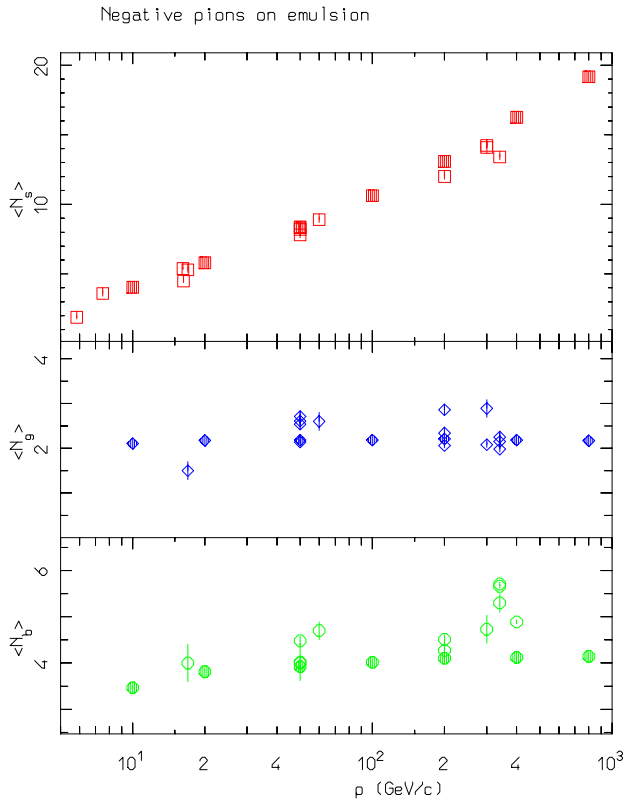

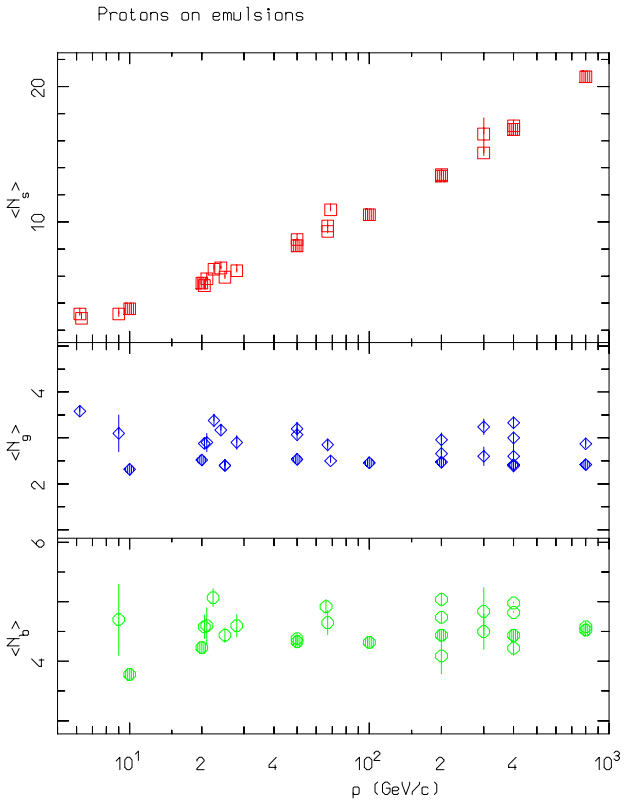

Shower, grey, and black tracks multiplicities for π^- (left) and protons (right) incident on emulsion, as a function of the projectile momentum. Open symbols are experimental data from various sources, full symbols are FLUKA results.

Nonelastic hA interactions at high energies: examples II

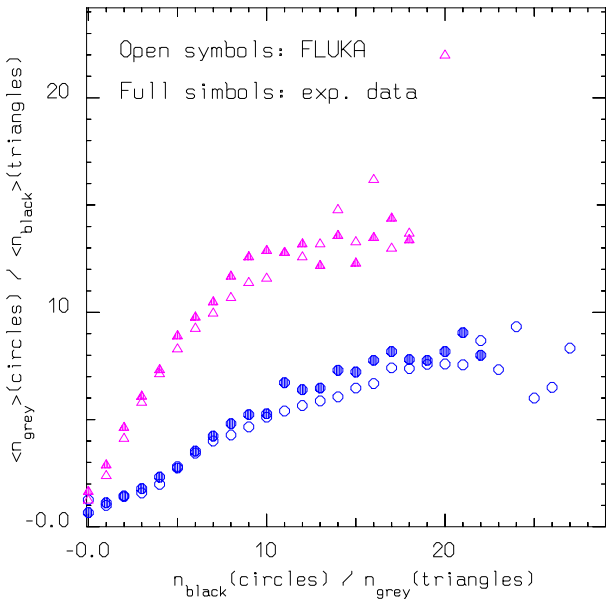

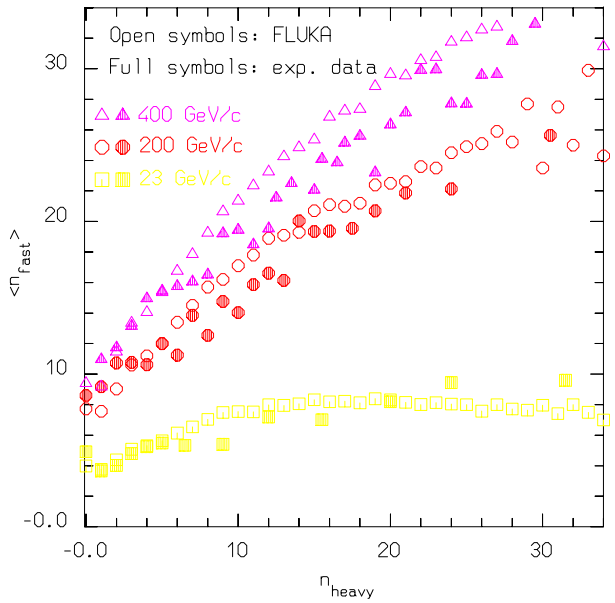

Correlation between the number of heavy prongs and fast particle multiplicity for protons on emulsion at various momenta, and mutual correlations ($< n_g >$ vs n_b and $< n_b >$ vs n_g) between black and grey charged tracks for 400 GeV/c p on emulsion. Open symbols are experimental data from various sources, full symbols are FLUKA results.

Residual nuclei: a test of evaporation and binding energy losses predictions

The production of residuals is a powerful check about the correctness of intranuclear cascading and the slow stages of hadronic interactions

The predictions about production of specific isotopes have additional problems wrt the calculation of emission spectra

- Small changes in the final evaporation steps can lead to fairly different residuals with little or no impact on the emitted spectra
- Nuclear structure effects play a major role which cannot be easily accounted for
- The lack of spin-parity dependent calculations in most MonteCarlo models limits their accuracy
- Fragmentation processes are known to populate the mass range A<20-30 for medium/heavy target nuclei. These processes are difficult to model in MonteCarlo codes.
- Isomer production: an open question
- The range of interesting cross section values typically spans *four* order of magnitudes

Fortunately for calorimetry purposes the residual mass distribution is a proper index of reliability, since there is no interest in specific isotope production

Residual nuclei: the mass distribution at high energies

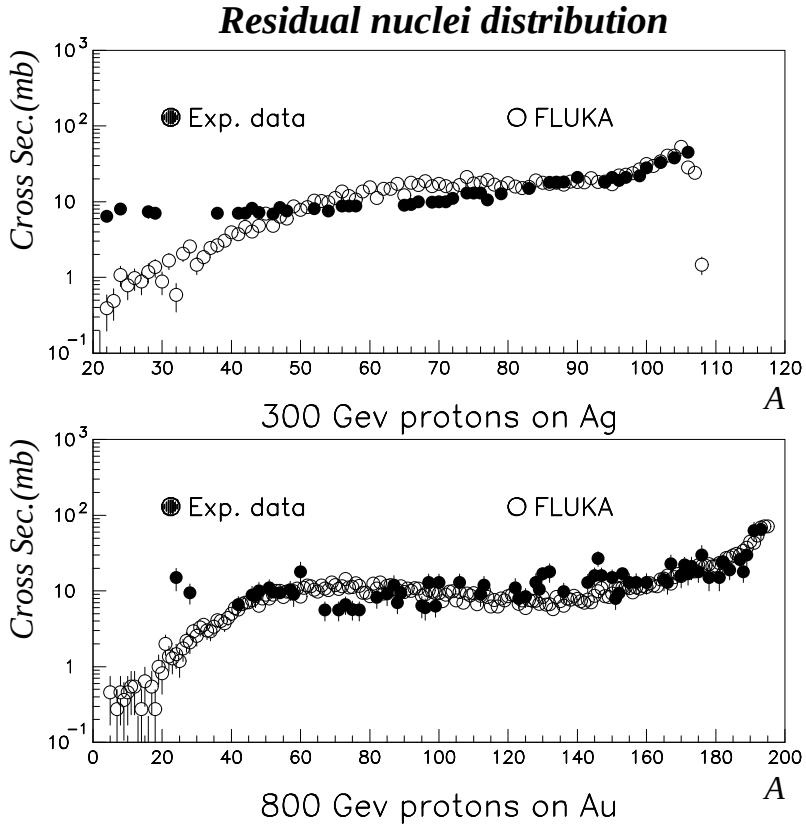

Experimental and computed residual nuclei mass distribution following for Ag(p,x)X at 300 GeV (top) and Au(p,x)X at 800 GeV (bottom).

Residual nuclei predictions: a look at the isotope table

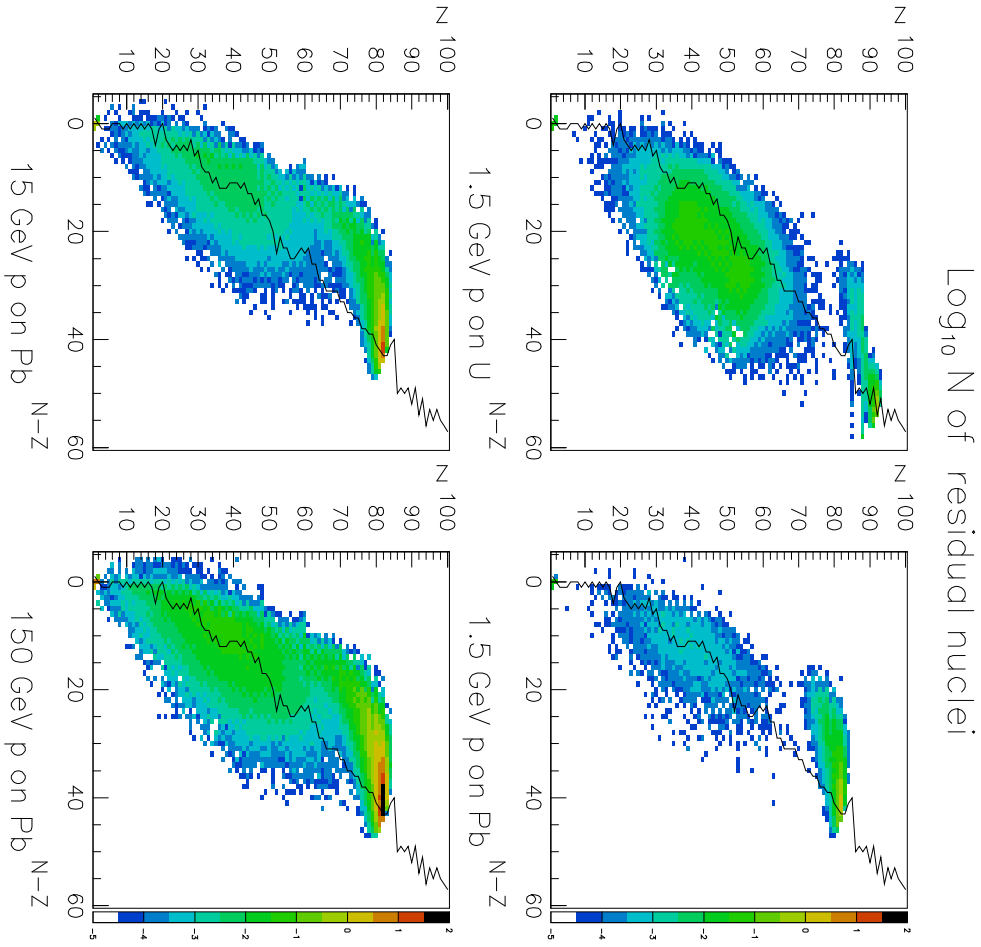

Low-medium energy h-A interactions: examples

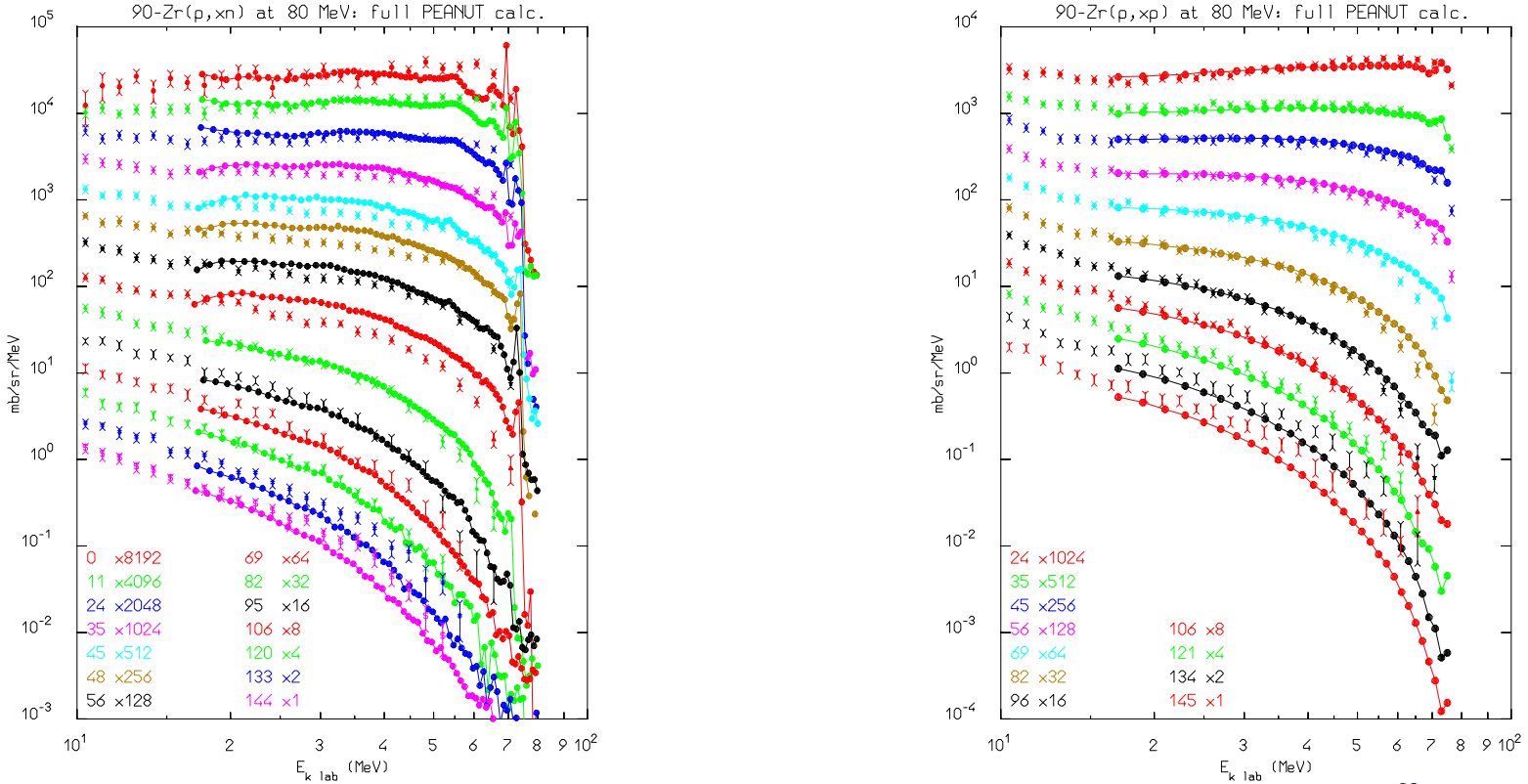

Computed (light symbols) and experimental (symbols with lines) double differential distributions for ^{90}Zr(p,xn) (left) and ^{90}Zr(p,xp) at 80.5 MeV. The exp. data have been taken from M.Trabandt et al. **PRC39** (1989) 452 and A.A. Cowley et al., **PRC43**, (1991) 678

Low-medium energy h-A interactions: examples II

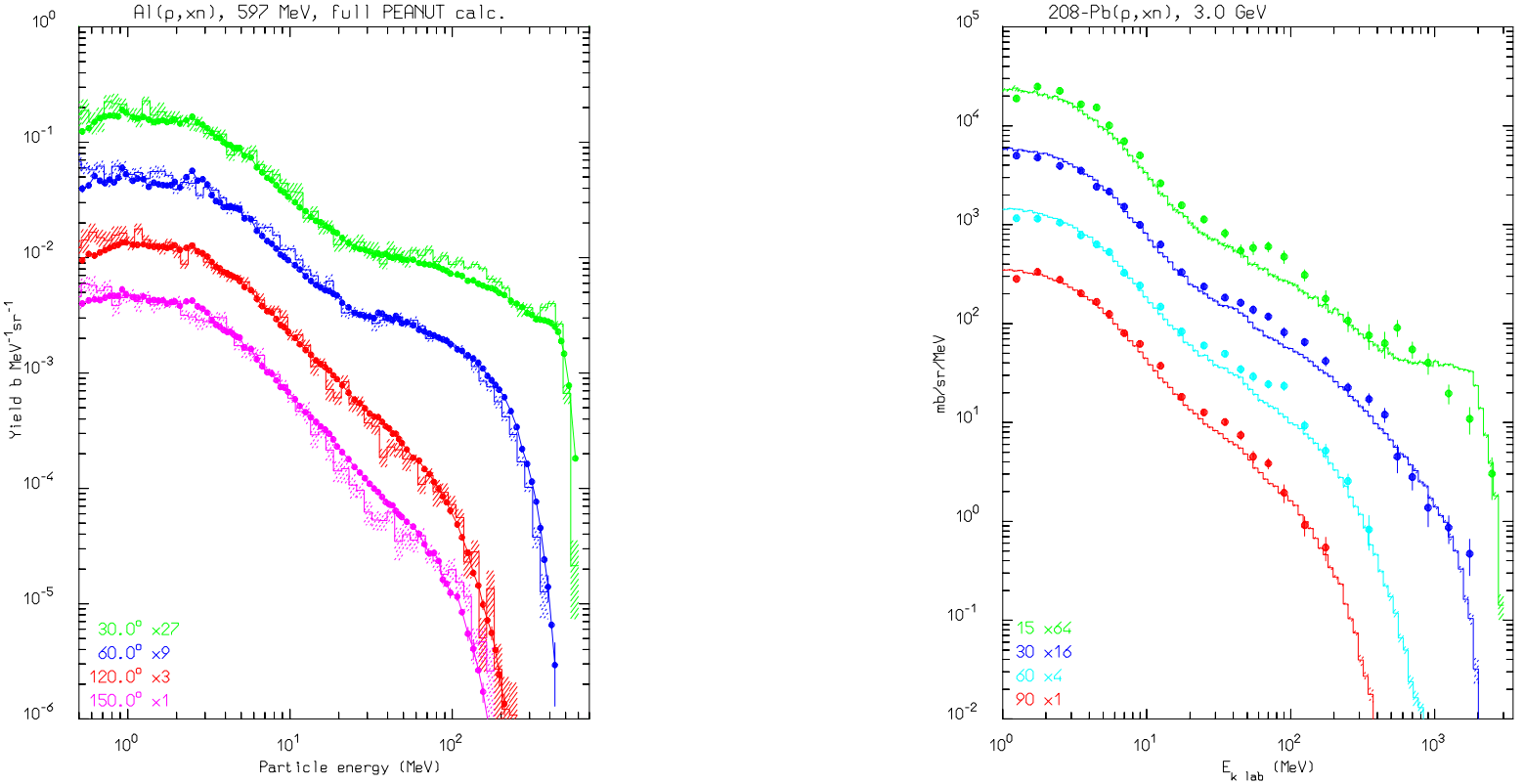

Computed (histograms) and experimental (symbols) double differential neutron distributions for Al(p,xn) (left) at 597 MeV and Pb(p,xn) at 3 GeV. The exp. data have been taken from W.B. Amian et al., Nucl. Sci. Eng. **115**, (1993) 1, and K. Ishibashi et al, Nucl. Sci. Technol. **32** (1995) 827.

Energy conservation and its relevance for sound calorimetric calculations

A fraction of the incoming energy in hadronic interactions is spent via mass production. Binding energy losses and their fluctuations are indeed an important ingredient, particularly at low projectile energies, both in determining the e/h ratio and the intrinsic resolution for hadronic showers.

A precise calculation of such losses can be easily performed using self-consistent interaction models fulfilling the basic conservations laws, energy, momentum and additive quantum numbers:

$$E_{k\ proj} + m_{proj} + {}^{A}_{Z}M \;=\; \sum_i \left[E_{k\ i} + m_i\right] + \sum_j \left[E_{k\ j} + {}^{A_j}_{Z_j}M_j\right]$$

Assuming meson masses can be recovered and antibaryons will eventually annihilate:

$$E_{loss} \;=\; \sum_i \left[I_{bar\ i} \cdot m_i\right] + \sum_j \left[{}^{A_j}_{Z_j}M_j\right] - I_{bar\ proj} \cdot m_{proj} - {}^{A}_{Z}M$$

$$I_{bar\ diff} \;=\; A - \sum_j A_j = \sum_i I_{bar\ i} - I_{bar\ proj}$$

It turns out that (obviously):

$$E_{loss} \;\approx\; 8 \times I_{bar\ diff}\ \mathrm{MeV}$$

Energy conservation: examples

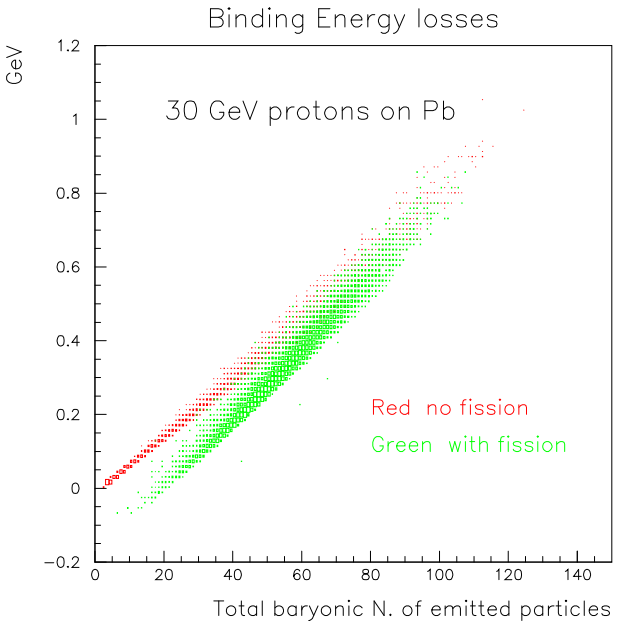

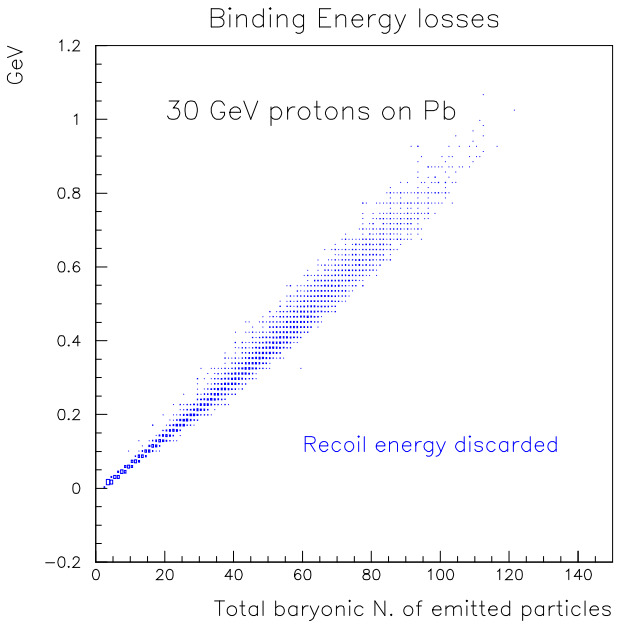

Binding energy losses for 30 GeV protons on lead (left). Binding energy losses plus heavy recoil energy for the same reaction (right)

The importance of in flight pion absorption

Both positive and negative pions can be absorbed in flight through multi-nucleon processes in nuclei. These processes are particularly important at subGeV energies

$\Downarrow$

- Competition with charge exchange strongly reduces the EM component
- Weakly ionizing relativistic particles are converted into heavily ionizing protons and energetic neutrons $\rightarrow$ signal losses

This process impacts the e/h ratio at all energies as well as resolutions at low-medium energies. It is critical for Cerenkov calorimeters

Microscopic pion absorption cross sections

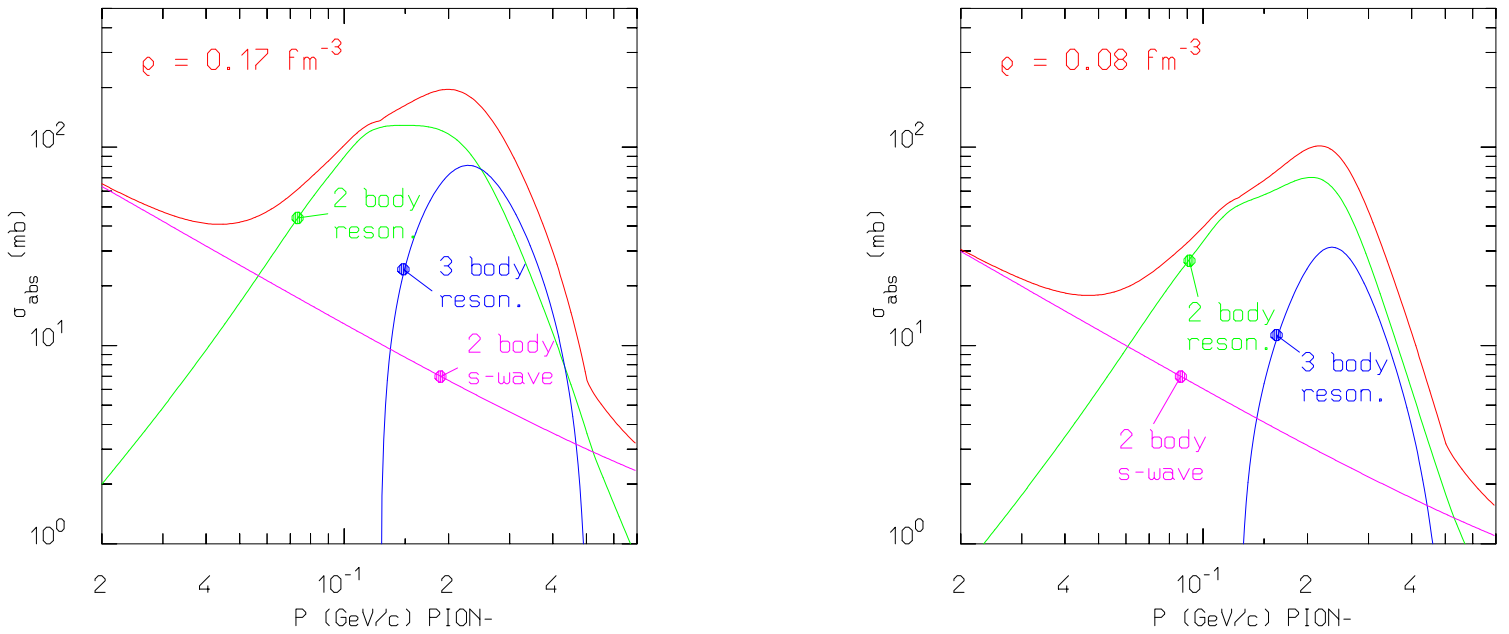

Charged pion absorption cross section for infinite symmetric nuclear matter at two different density values ($\lambda_{abs}^{-1} = \sigma_{abs} \cdot \frac{1}{2}\rho = \sigma_{abs} \cdot \rho_{pro} = \sigma_{abs} \cdot \rho_{neu}$)

Pion absorption cross sections: examples

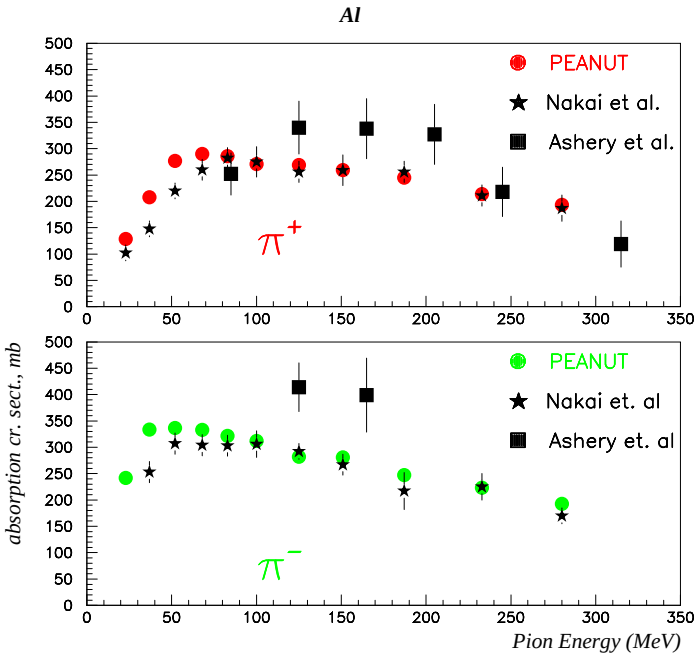

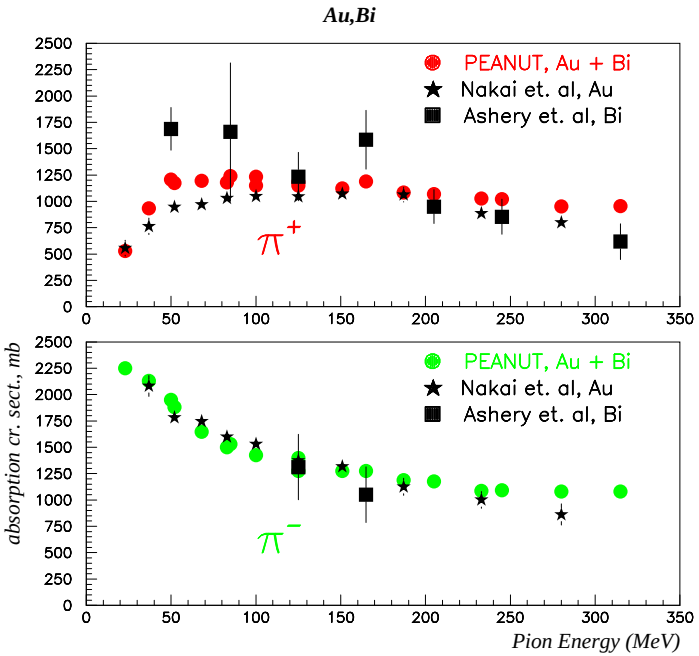

Computed and exp. pion absorption cross section on Aluminum as a function of energy

Computed and exp. pion absorption cross section on Gold or Bismuth as a function of energy

(Exp. data: D. Ashery et al., **PRC23**, (1981) 2173 and K. Nakai et. al., **PRL44**, (1979) 1446)

Quenching of heavily ionizing particle signals

An important contribution to calorimeter non compensation comes from *quenching/recombination* of signals (light, ionization...) in the sensitive medium.

A popular way to express the dependence of these effects on the ionization density is given by the Birks law:

$$\frac{dS}{d\rho x} = \left(\frac{dS}{dE}\right)_0 \frac{\frac{dE}{d\rho x}}{1 + K\frac{dE}{d\rho x} + ...}$$

Some typical values:

- K for organic scintillators: ≈0.0085–0.013 $(\mathrm{MeV/gr/cm^2})^{-1}$)
- K for LAr around 10 kV/cm: ≈0.005–0.007 $(\mathrm{MeV/gr/cm^2})^{-1}$)
- K for LAr around 400–500 V/cm: ≈0.11 $(\mathrm{MeV/gr/cm^2})^{-1}$)
- K for LAr around 400–500 V/cm with TMG doping: ≈0.05 $(\mathrm{MeV/gr/cm^2})^{-1}$)

Quenching of heavily ionizing particle signals: examples

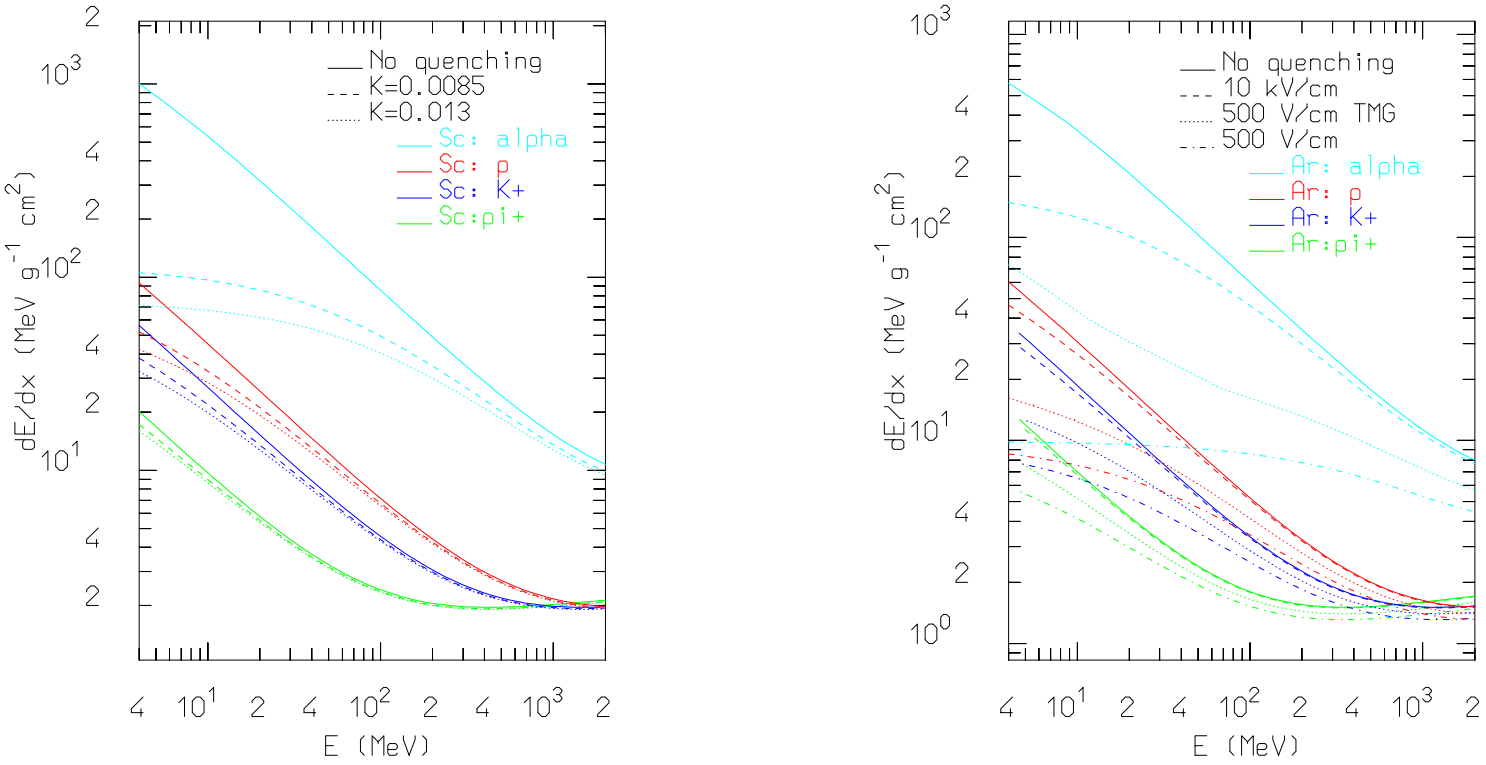

"Equivalent" stopping power for various particles in scintillator (left) and LAr (right) for some values of the quenching parameters

"Low" energy neutrons

The fraction of visible energy due to neutrons below 10-20 MeV is still very significant. Most of their kinetic is spent via elastic interactions.

Recoils are usually heavily quenched and a significant fraction of the energy is going into non ionizing recoils, except in the case of hydrogen.

Most of the low energy neutron contribution comes from capture γ rays. The capture probability is maximal in the thermal region: thermalization times can vary from μs to ms depending on the material composition

In principle if the capture γ ray contribution could be fully accounted for most of the binding energy losses would be recovered

"Low" energy neutrons: cross sections

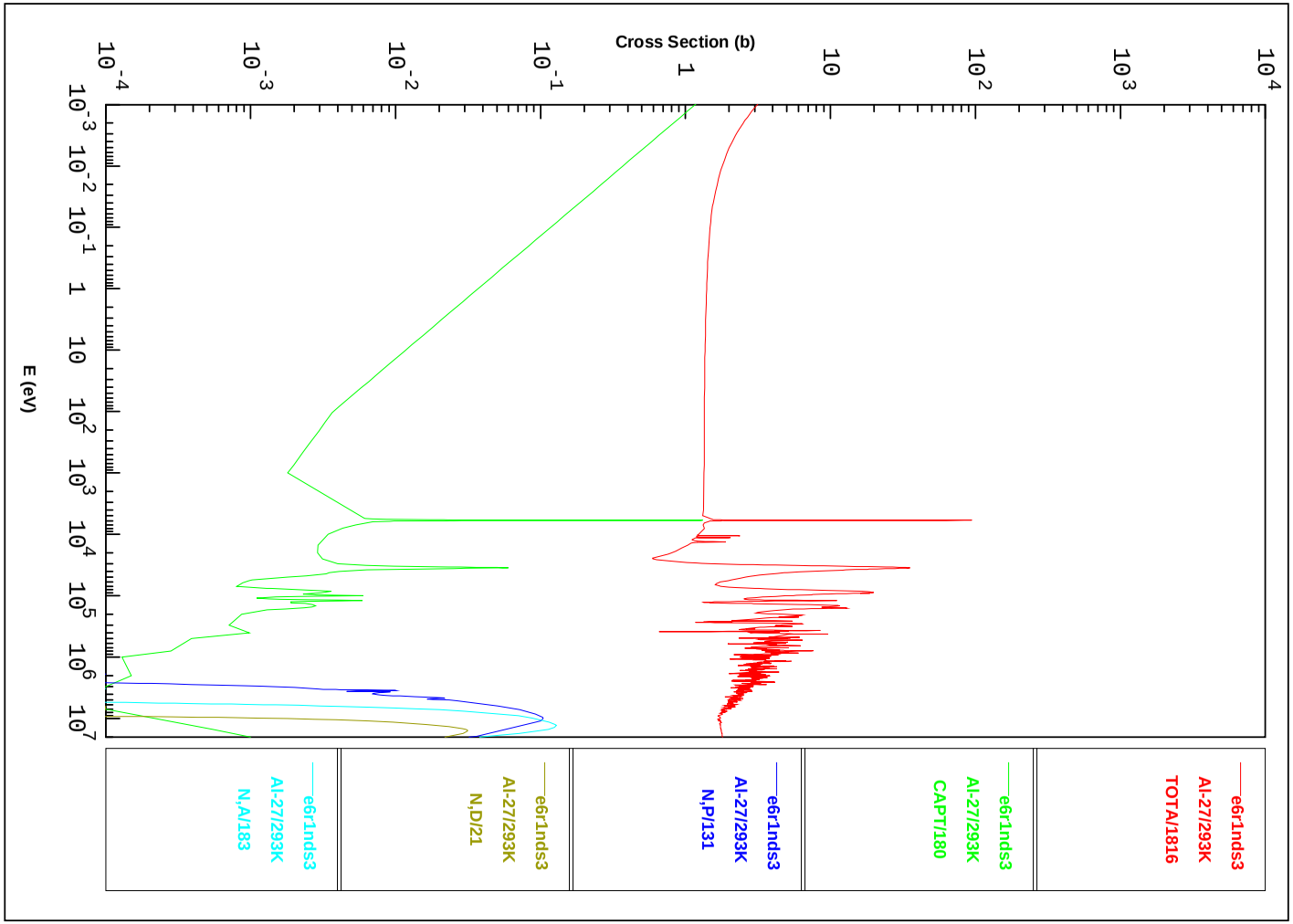

"Low" energy neutrons: cross sections

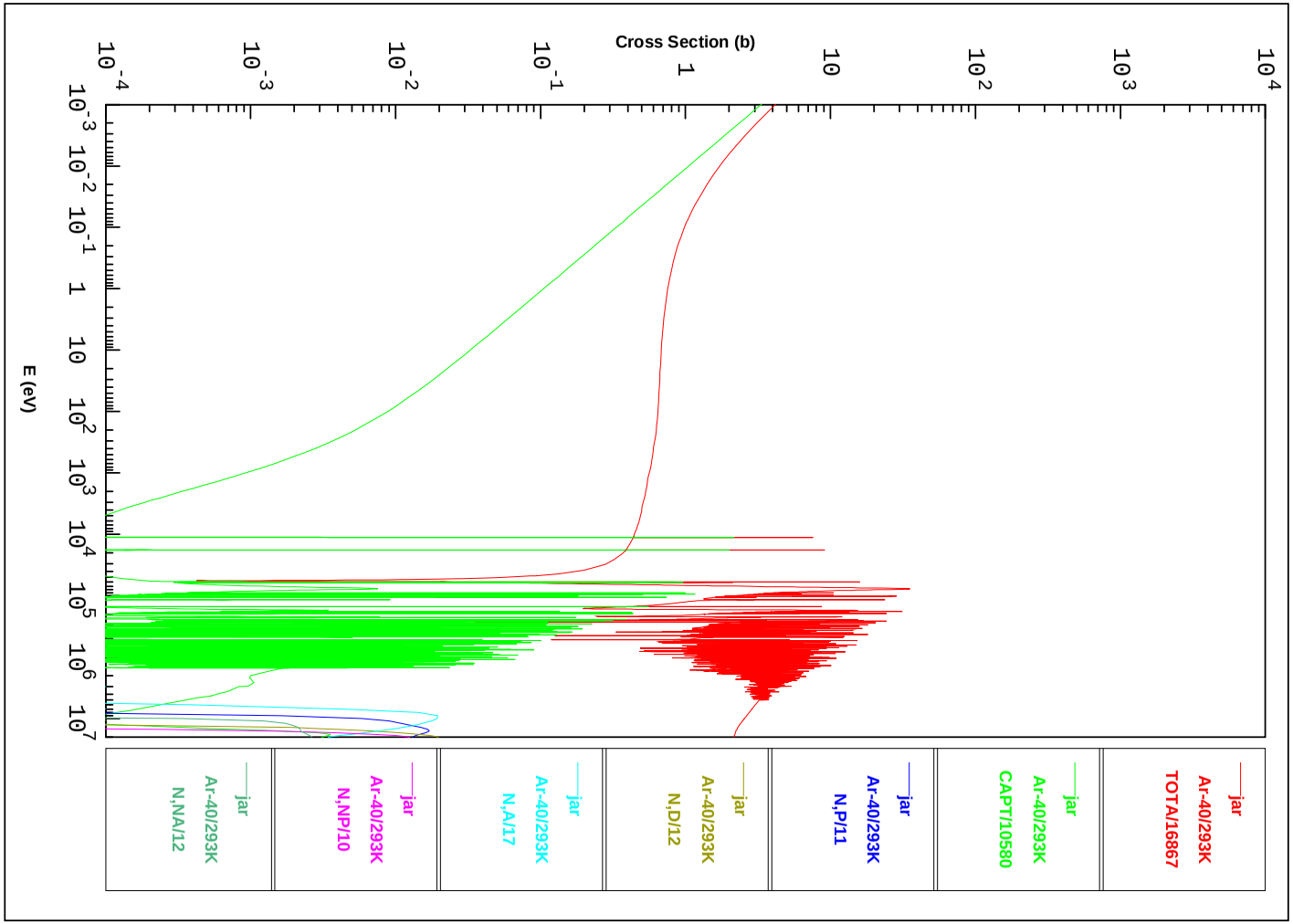

"Low" energy neutrons: cross sections

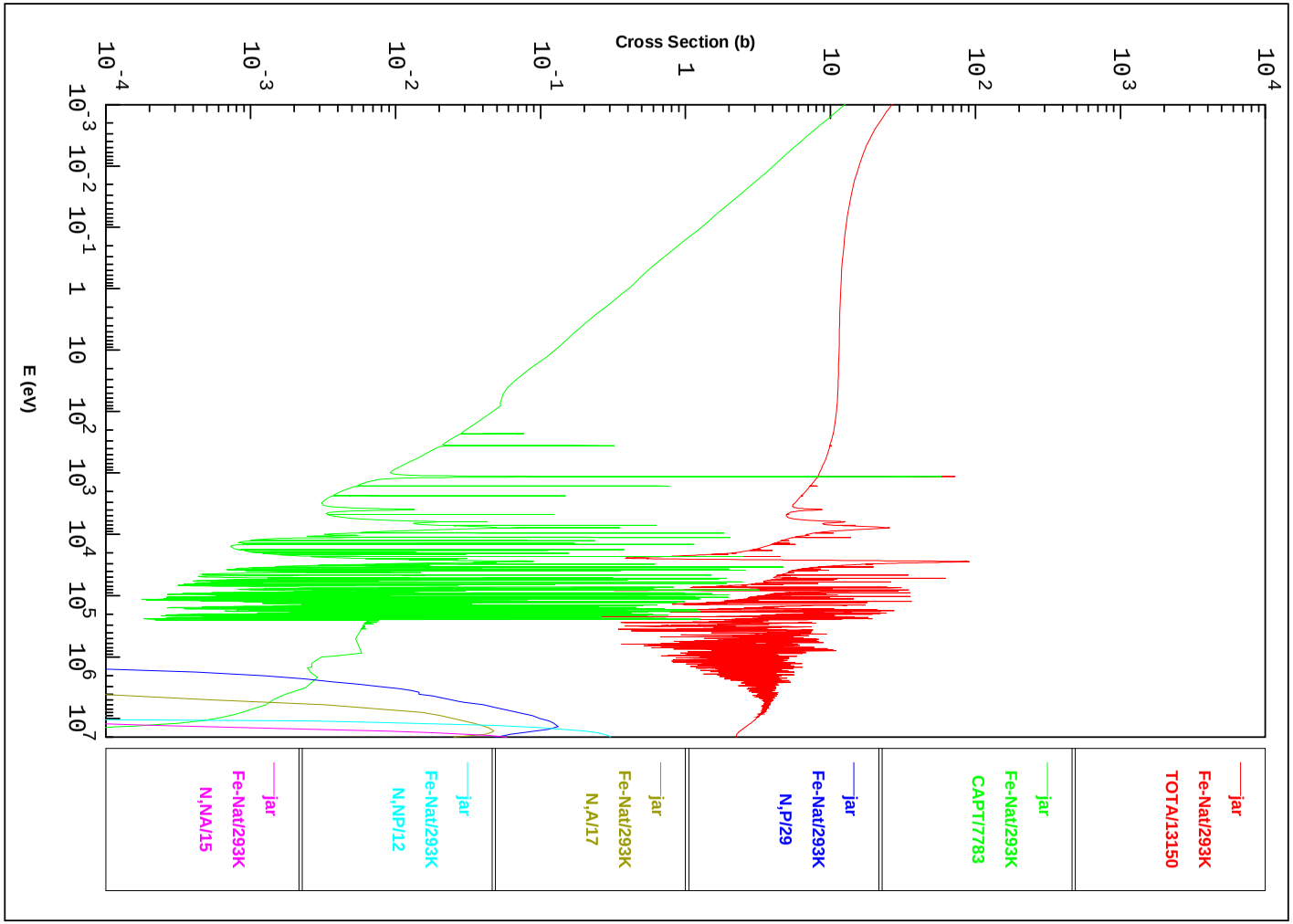

"Low" energy neutrons: cross sections

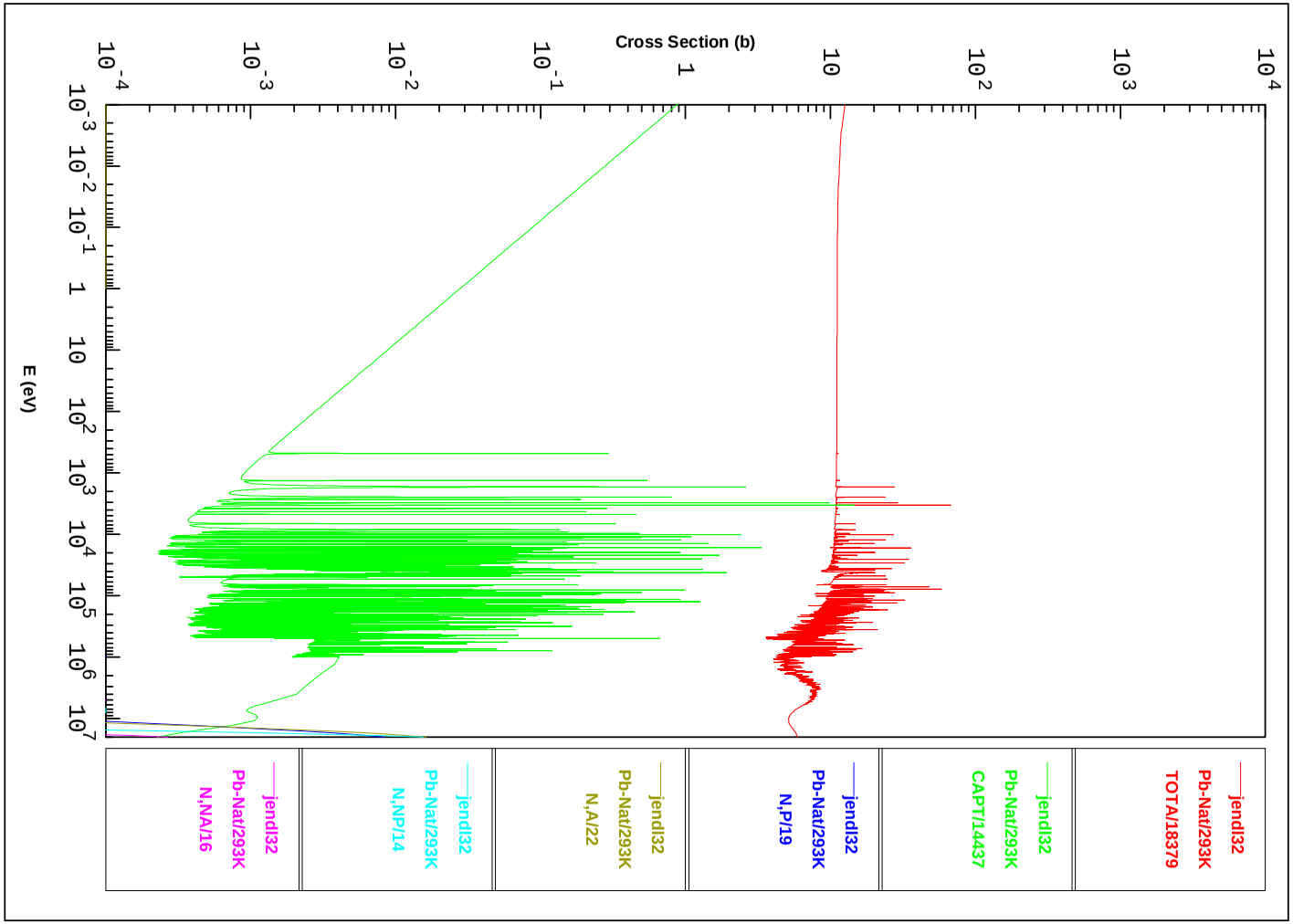

"Low" energy neutrons: cross sections

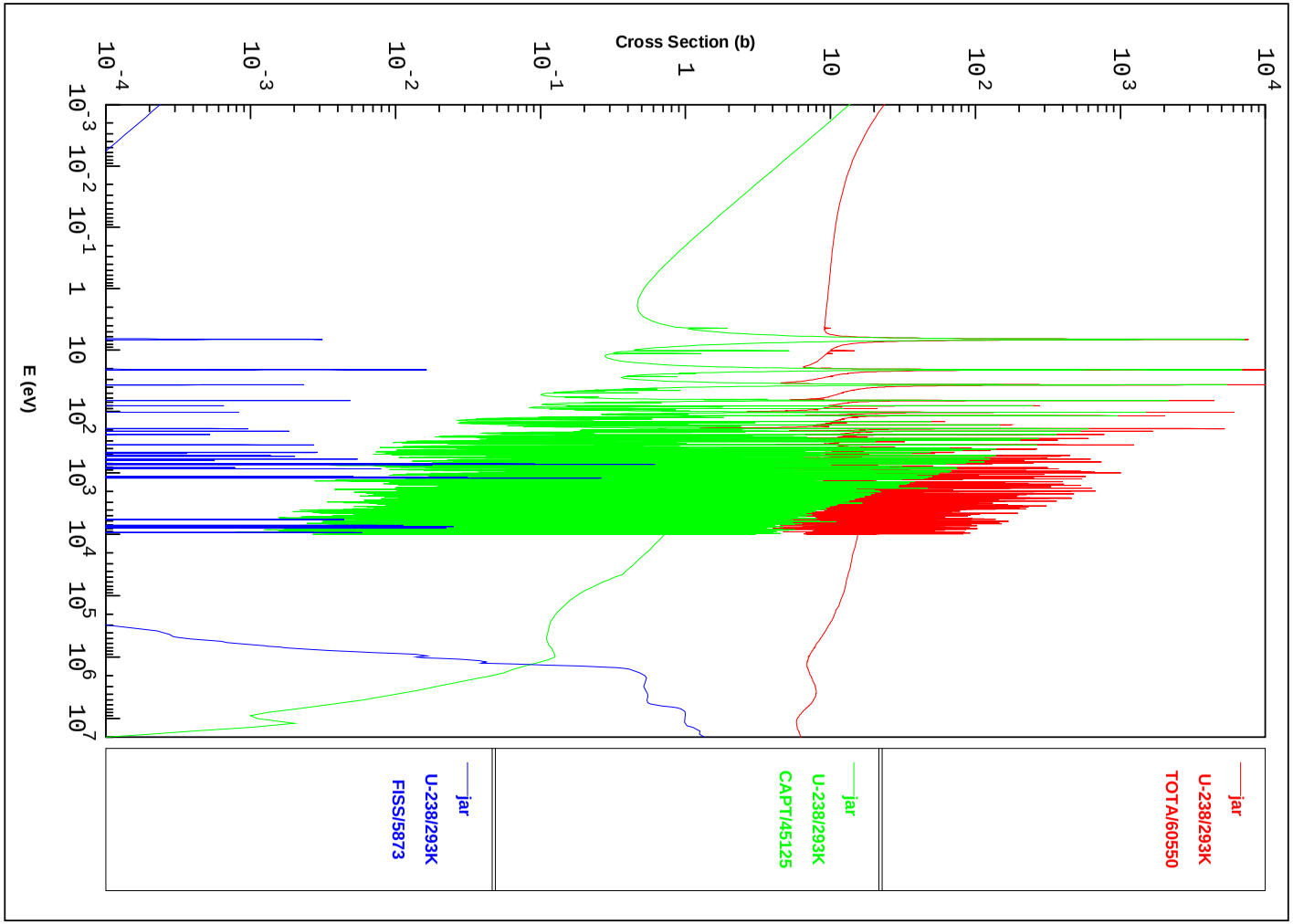

Neutron production examples: thick targets

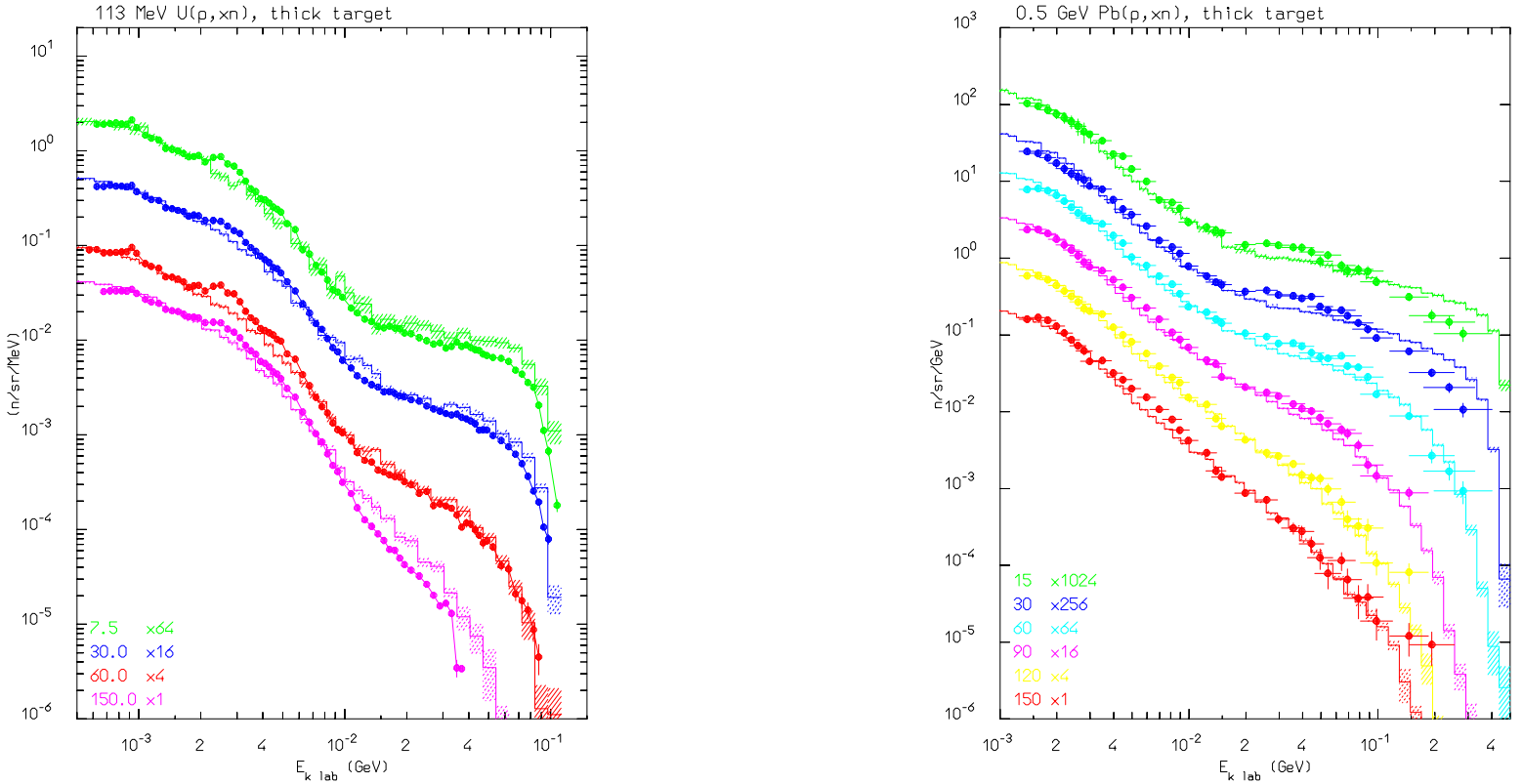

Simulated (dashed histogram) and experimental (symbols) neutron double differential distributions out of stopping length targets for 113 MeV protons on U (left, data from M.M. Meier et al., Nucl. Sci. Eng. **110**, (1992) 299) and 500 MeV protons on Pb and 256 MeV protons on uranium (right, S. Meigo et al., JAERI-Conf 95-008, (1995), 213)

Neutron production examples: TARC (PLB458 (1999) 167)

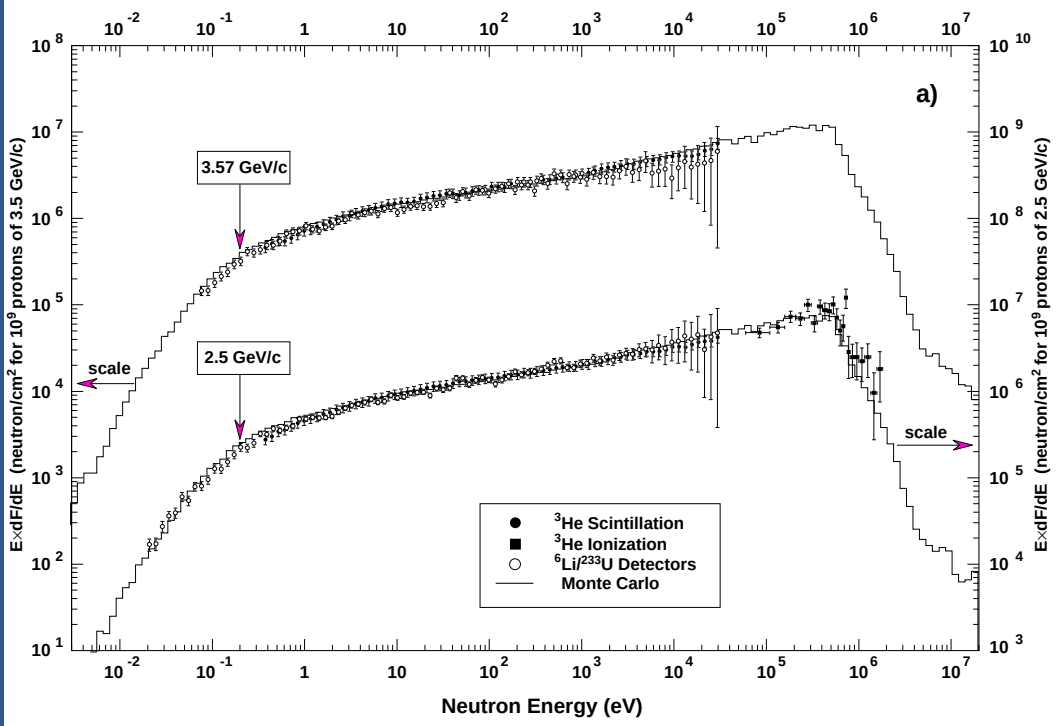

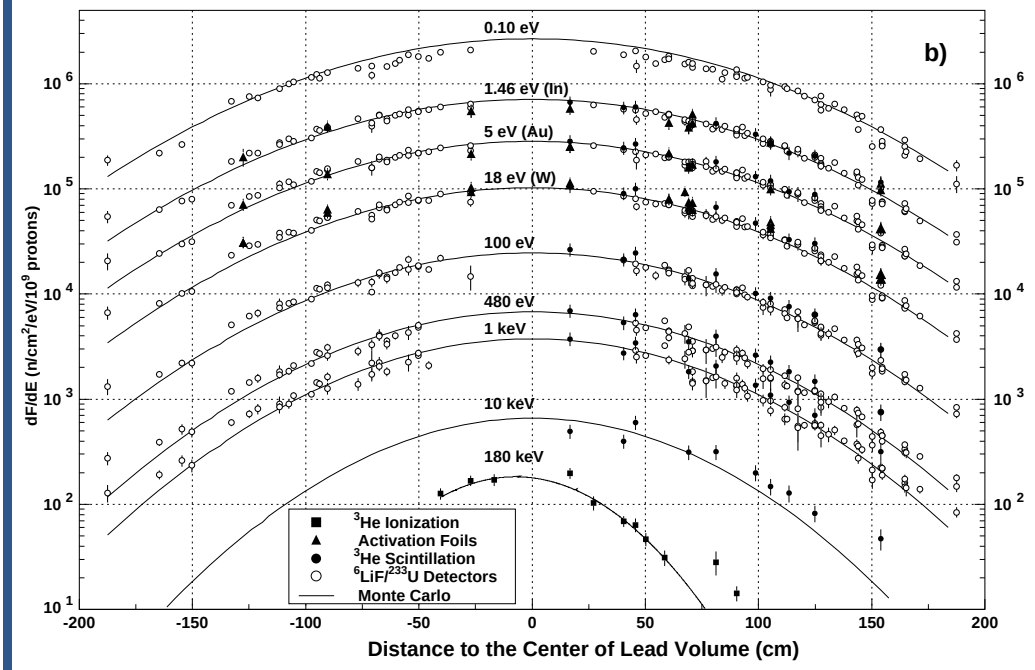

Infinite homogeneous calorimeters: some examples

Shower calculations at energies ranging from 1 to 300 GeV have been performed using infinite and homogeneous targets (Al, Fe, Pb and U)

The various contributions to a possible signal have been scored, together with the energy lost for binding and neutrinos.

In the following we will focus on the relative role of:

- The electromagnetic energy fraction
- The energy due to γ's produced by slow neutrons
- The energy spent in "heavy" (heavier than α's) recoils and fission fragments
- The energy lost due to binding

Infinite calorimeters: the electromagnetic component

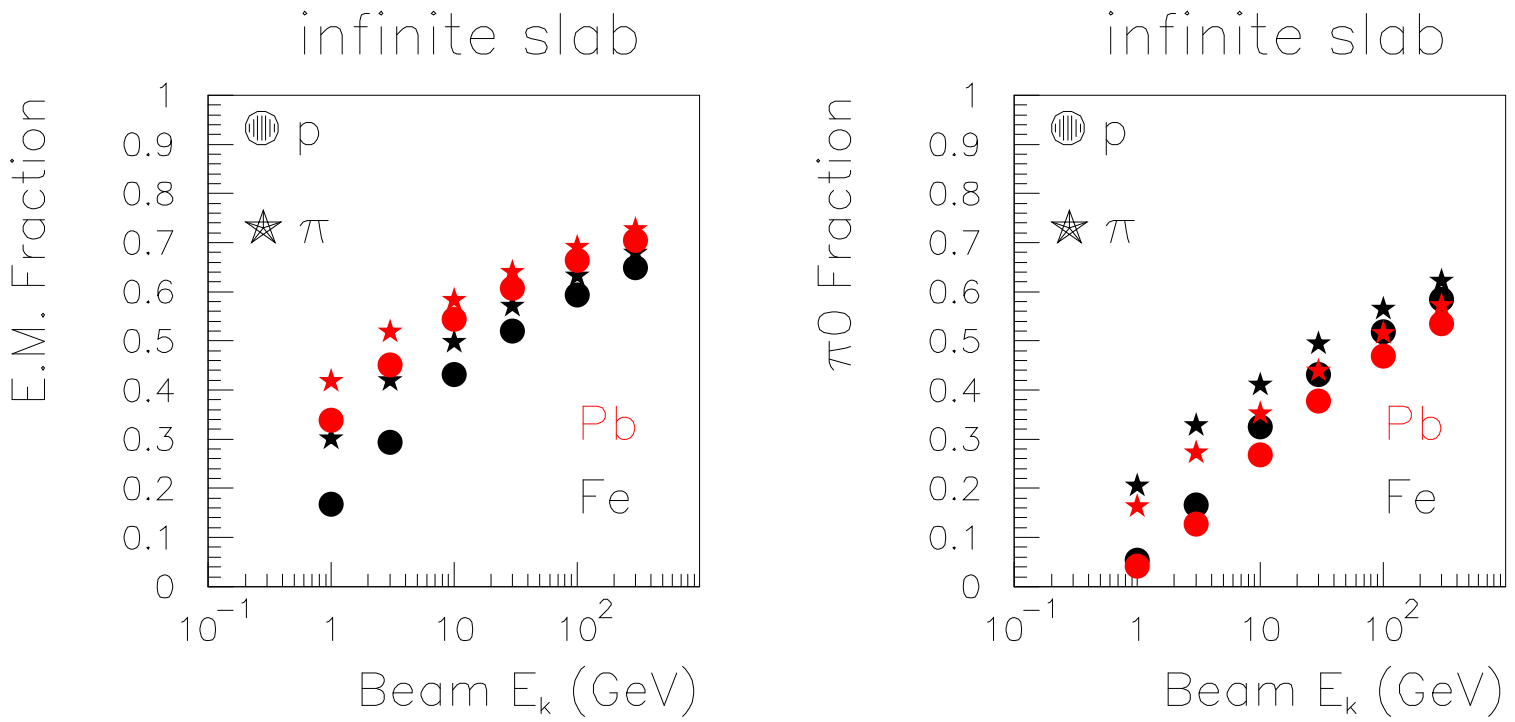

Energy fraction carried by π^0's and γ's for pion and proton showers (left). The same fraction without the slow neutron γ contribution (right)

Infinite calorimeters: binding losses

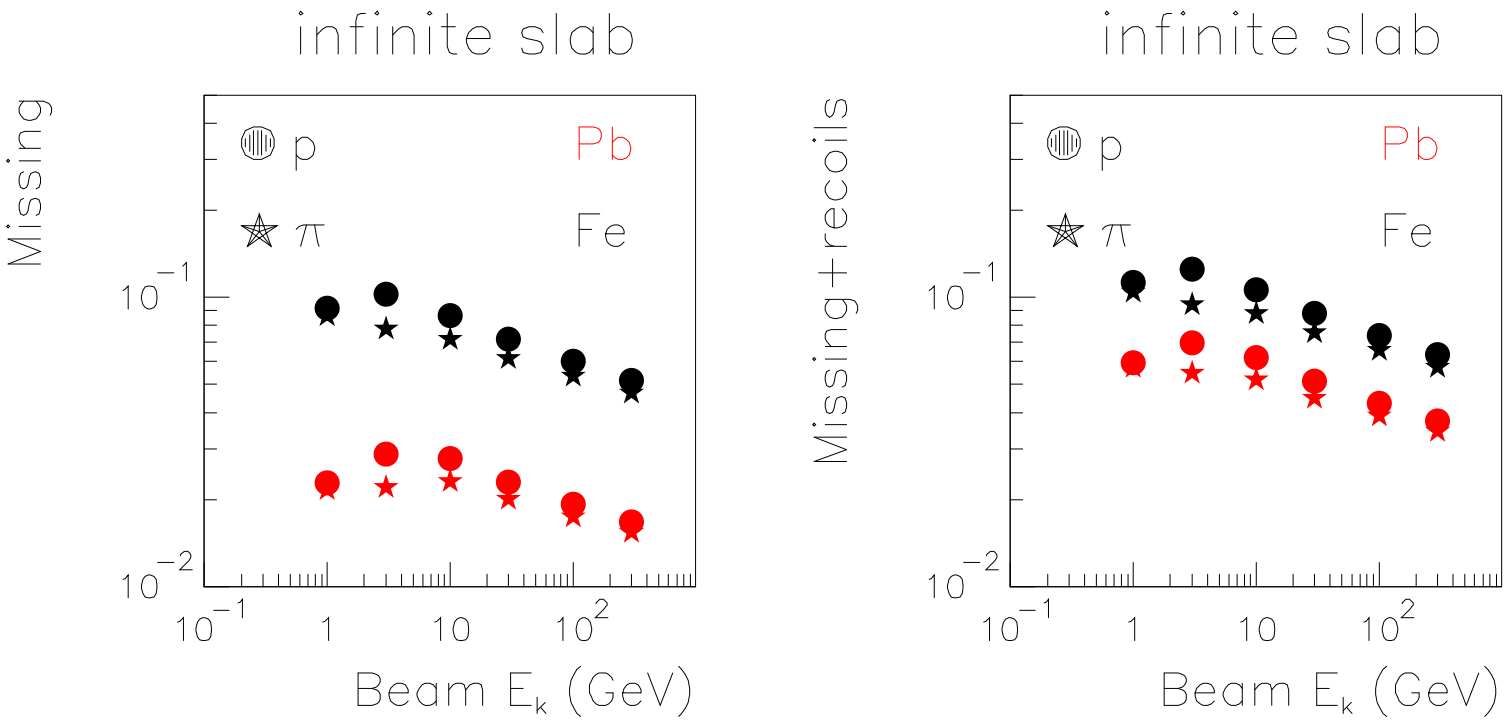

Average energy fraction "lost" due to binding for pion and proton showers (left). The same with in addition the energy due to heavy recoils and fission fragments (right)

Infinite calorimeters: the role of slow neutrons

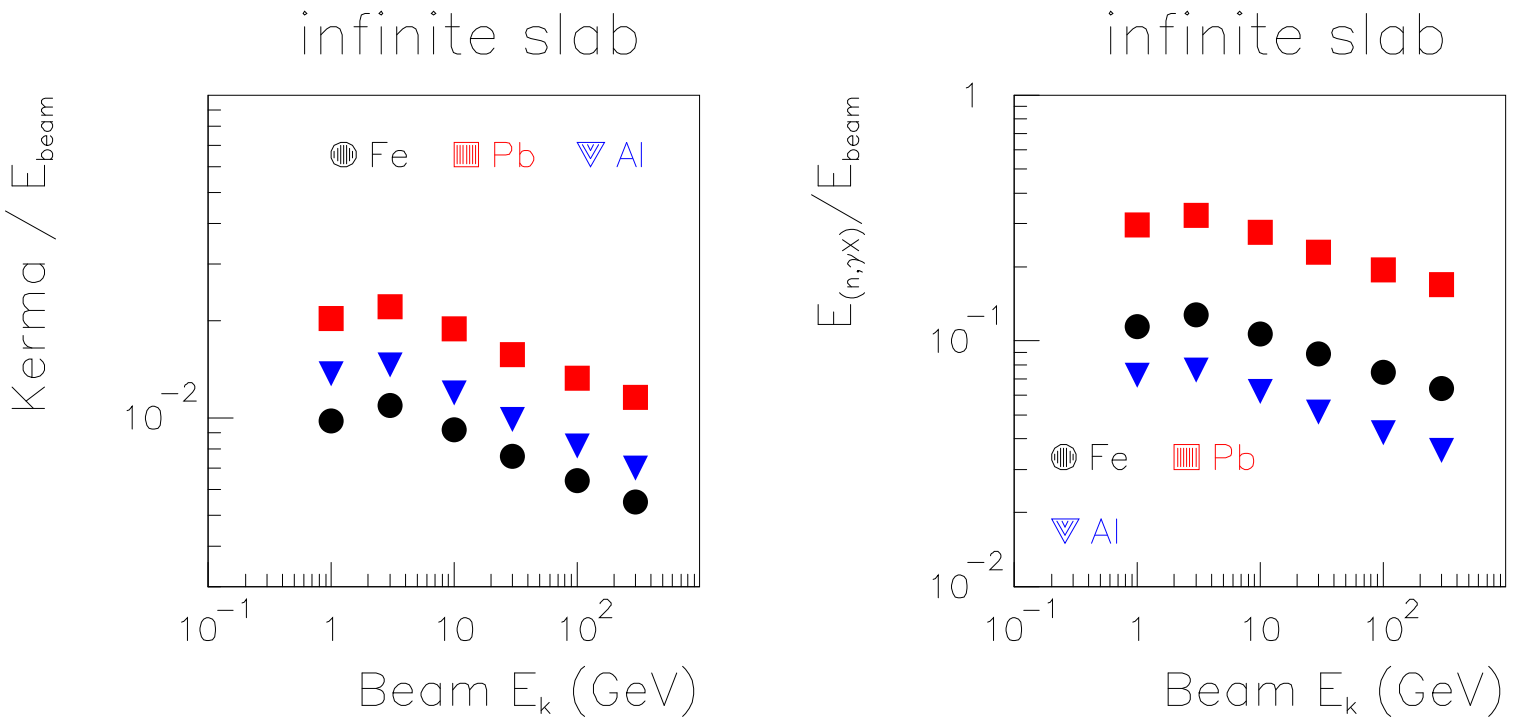

Average fractions of energy carried by "slow" neutrons, kinetic (left), and by γ's produced in (n,n') and capture reactions (right)

Infinite calorimeters: slow neutrons II

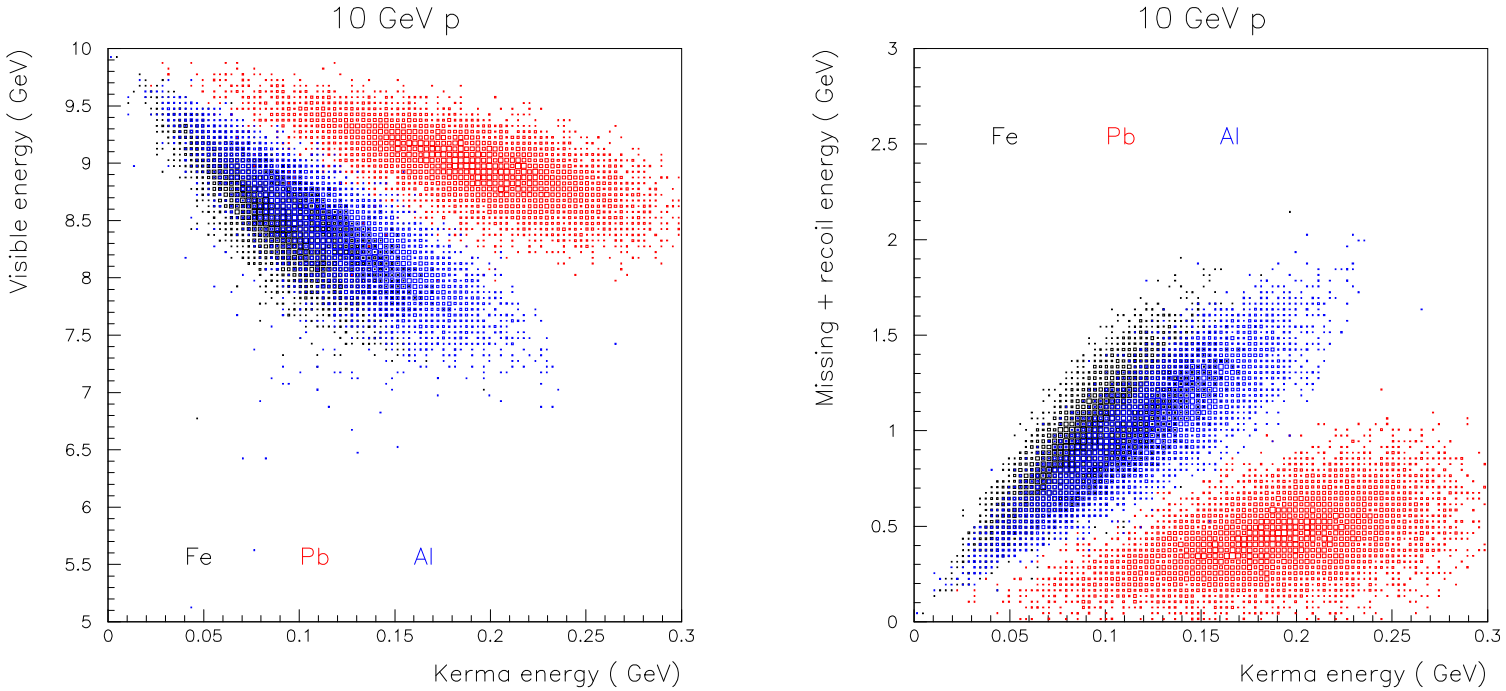

Correlation between slow neutron kinetic energy and (left) "visible" energy (everything but heavy recoils and fission fragments), (right) binding energy losses

Infinite calorimeters: slow neutrons III

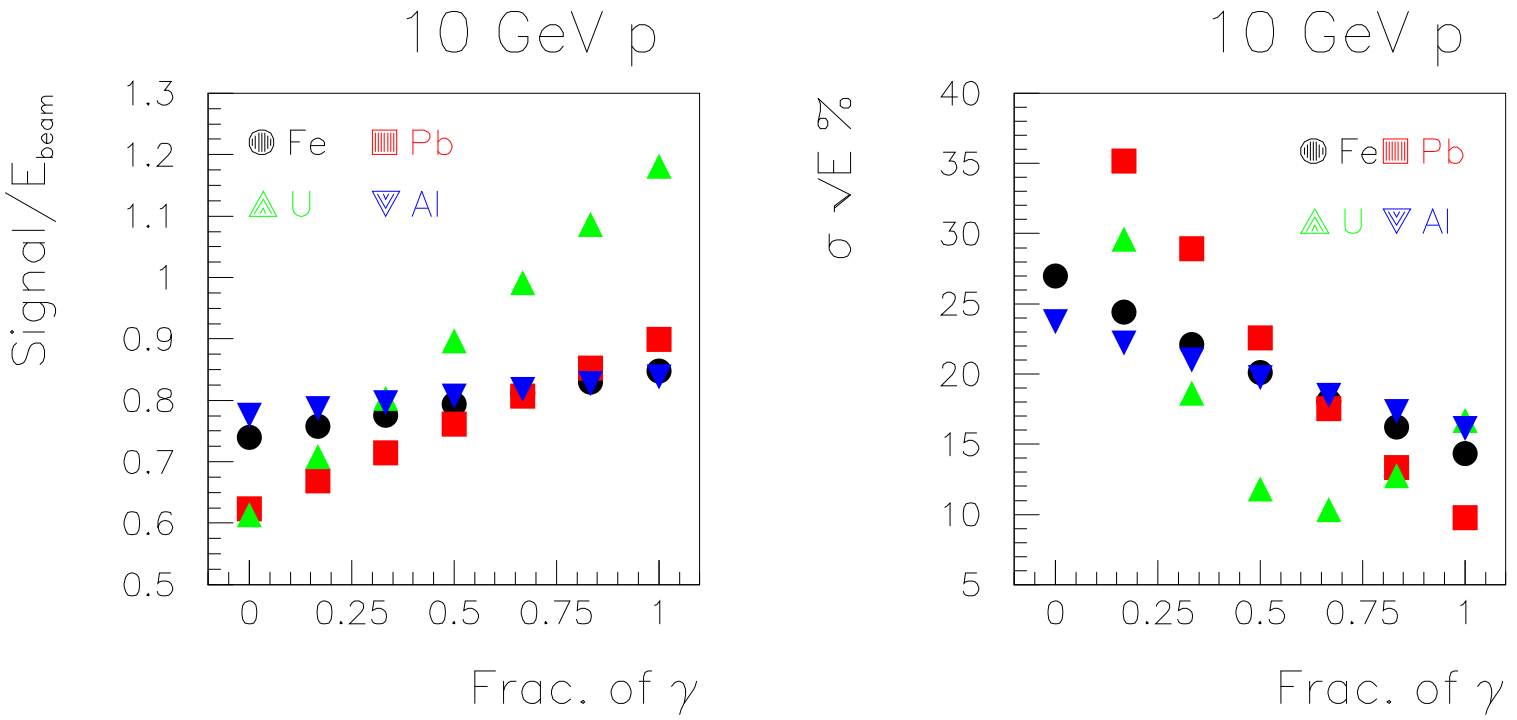

Average "visible" signal (left) (heavy recoil excluded, no quenching) and fractional resolution (right) as a function of the fraction of slow neutron γ's collected

Infinite calorimeters: slow neutrons IV

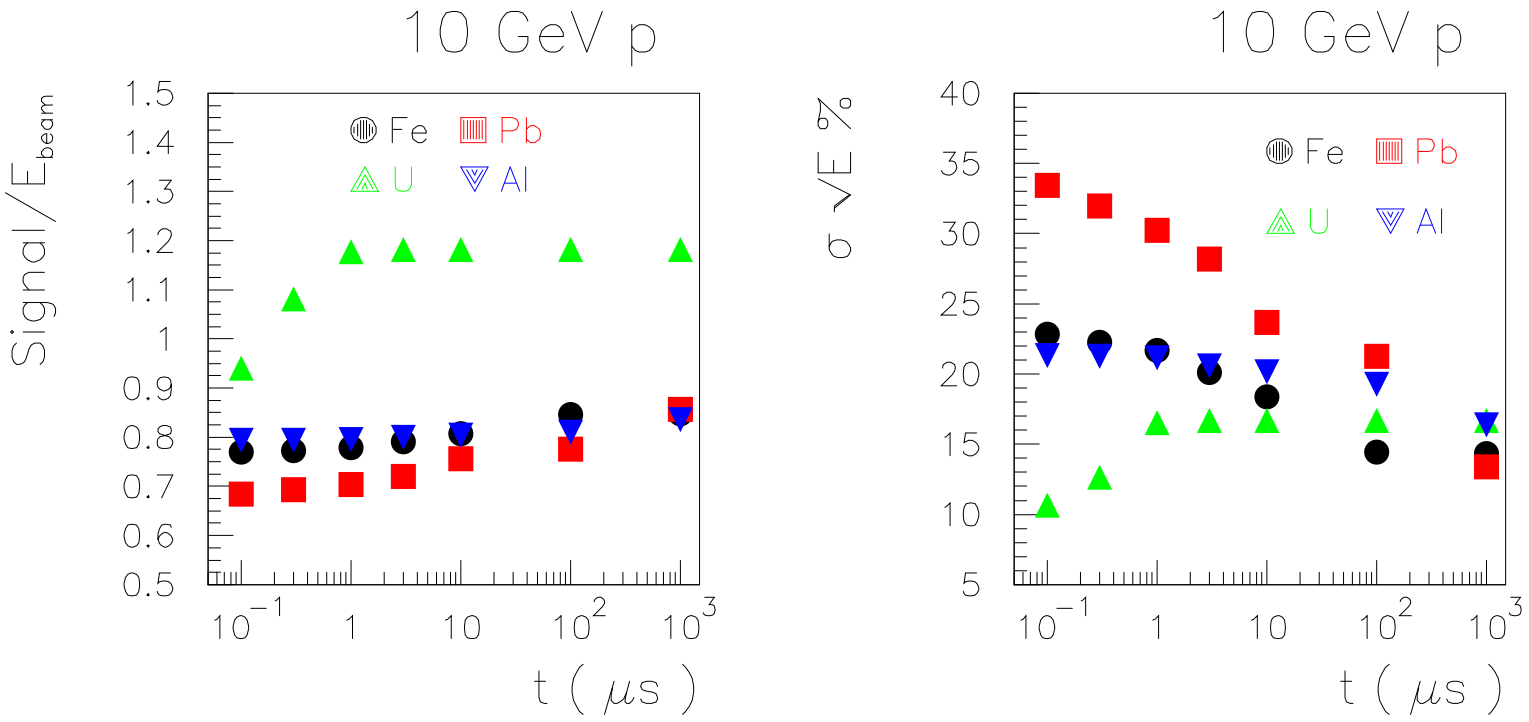

Average "visible" signal (left) (heavy recoil excluded, no quenching) and fractional resolution (right) as a function of integration time. *The time scales are meaningful only for the given materials, hydrogen content could significantly affect neutron thermalization times*

Infinite calorimeters: slow neutrons V

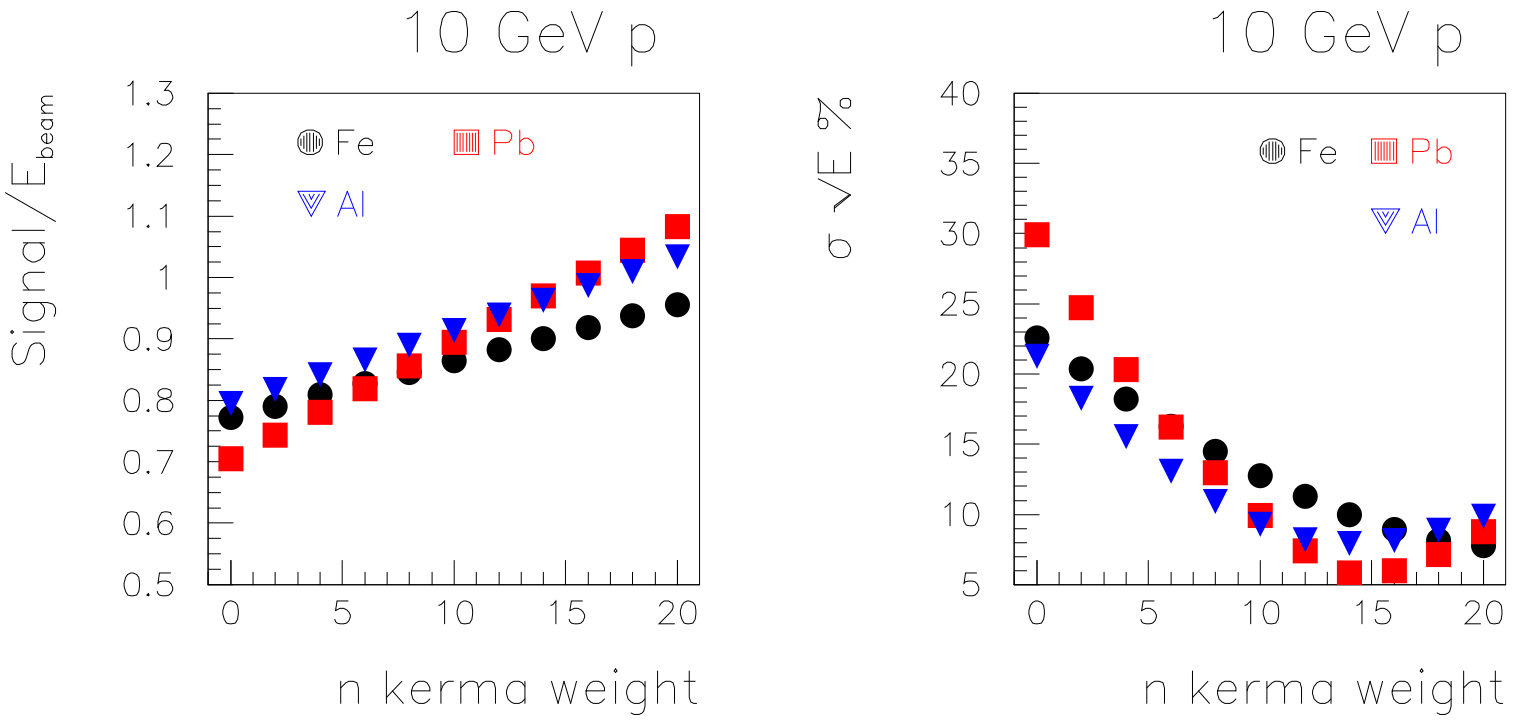

Average "visible" signal (left) (heavy recoil excluded, 30% of neutron produced γ's, no quenching) and fractional resolution (right) as a function of the enhancement of the slow neutron kinetic energy signal (i.e. using hydrogen in the sensitive medium)

ICARUS liquid argon imaging TPC (I)

- The LAr TPC technique is based on the fact that ionization electrons can drift over large distances (meters) in a volume of purified liquid Argon under a strong electric field. If a proper readout system is realized (i.e. a set of fine pitch wire grids) it is possible to realize a massive "electronic bubble chamber", with superb 3-D imaging.

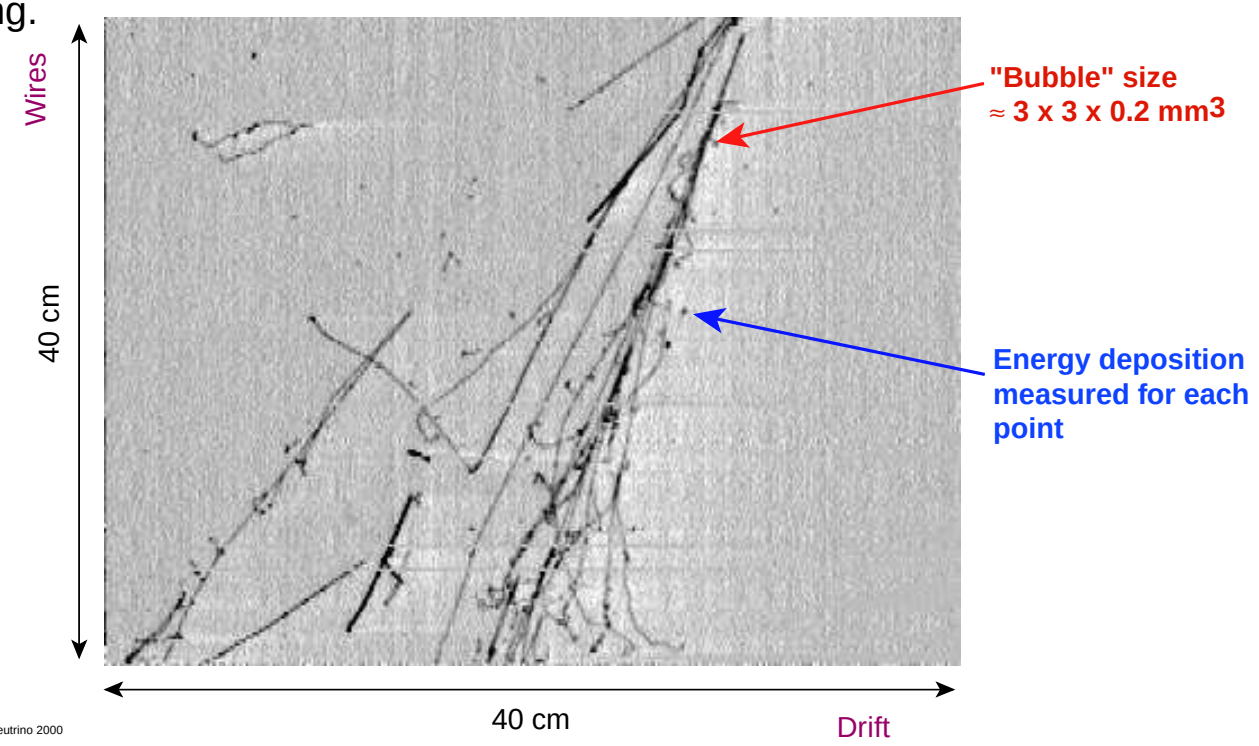

Calorimetry in imaging, fully sensitive liquid Argon

Liquid argon is a non-compensating medium. When used in a time projection chamber like ICARUS the effect is exacerbated by the relatively low electric field ($\approx$ 300–500 V/cm)

However, the medium appears as a *completely homogeneous volume with very high readout granularity*

$\Downarrow$

From the event visualisation and from the local charge deposition density, it is possible both to distinguish between electromagnetic and hadronic components of a shower and to approximately correct for the recombination effects.

Calorimetry in imaging, fully sensitive liquid Argon

Quenching correction

Let assume that each elementary cell contains only one crossing track, the recombination effect can be unfolded using the collected charge and cell width to construct the observed dQ/dx and solving the recombination expression for the "actual" dE/dx. *Despite its simplicity, the procedure is very effective in recovering most of the recombination, particularly when the Argon is doped with TMG*

Compensation correction

Let us assume that electromagnetic energy deposition can be distinguished from hadronic one, the total energy of a shower is obtained as the sum of two terms $E = w \times (Q_{em} + \alpha \times Q_{had})$, where α is the compensation factor. *For pure argon,* α *is about* 1.5 (2.8) *with and without quenching corrections respectively. The same figures for TMG-doped argon are* 1.5 *and* 2.0

ICARUS: resolutions for pions

Expected hadronic resolution for pions

Medium	Compensation	Quench corr.	Resolution
Pure argon	no	no	$27\%/\sqrt{E} \oplus 8\%$
	yes	no	$24\%/\sqrt{E} \oplus 4\%$
	no	yes	$18\%/\sqrt{E} \oplus 6\%$
	yes	yes	$16\%/\sqrt{E} \oplus 1\%$
TMG doped argon	no	no	$20\%/\sqrt{E} \oplus 6\%$
	yes	no	$16\%/\sqrt{E} \oplus 2\%$
	no	yes	$15\%/\sqrt{E} \oplus 5\%$
	yes	yes	$12\%/\sqrt{E} \oplus 0.2\%$
No quenching	no	–	$15\%/\sqrt{E} \oplus 5\%$
	yes	–	$12\%/\sqrt{E} \oplus 0.1\%$

Expected resolution in the liquid target for pions with and without TMG doping, showing the effect of the offline compensation and quench correction. For reference, the resolution that would be obtained with no recombination effects is also listed.

ATLAS combined calorimeter test beam

Layout of the experimental set-up (NIM A387,333(1997), NIM A449,461 (2000))

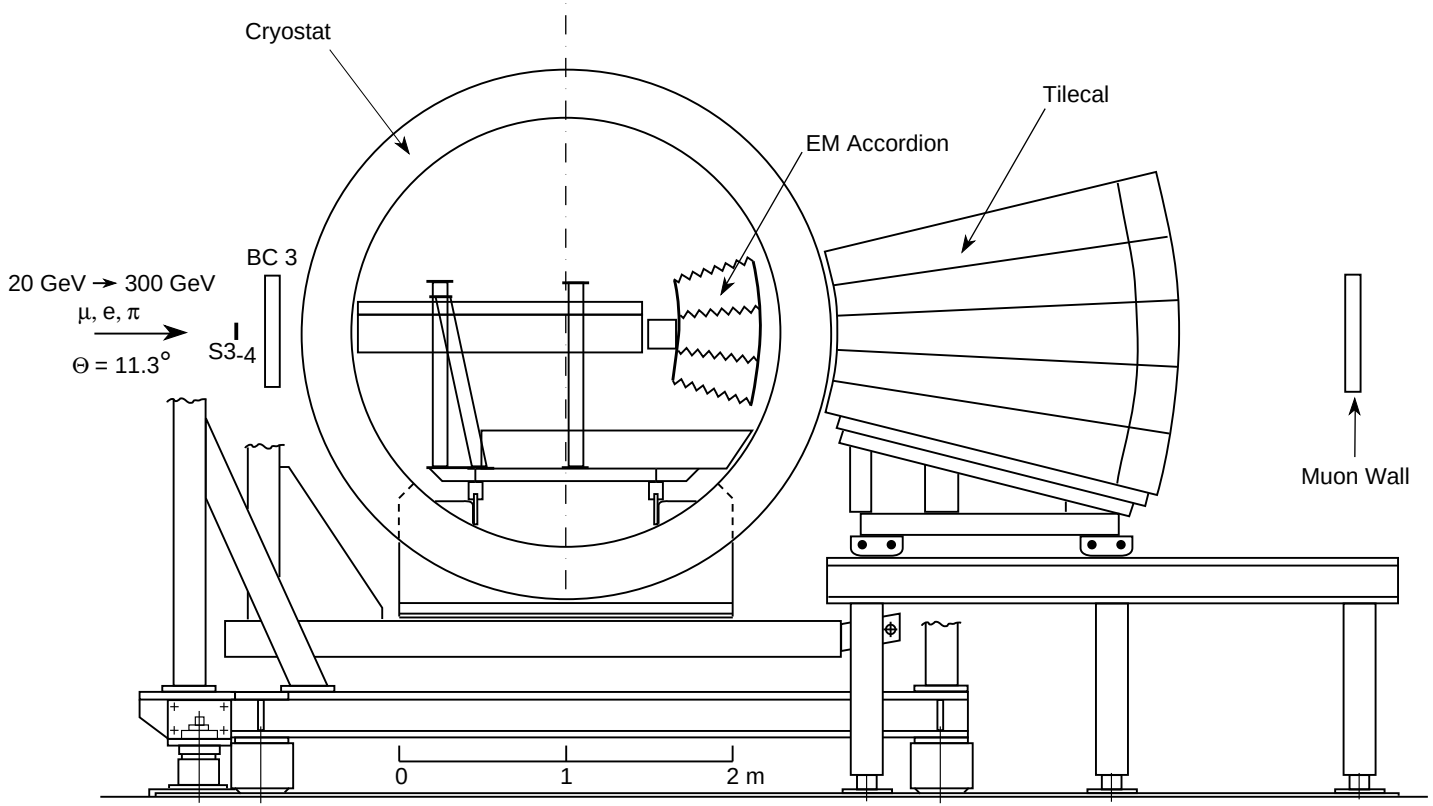

LAr electromagnetic calorimeter

Detail of the accordeon structure

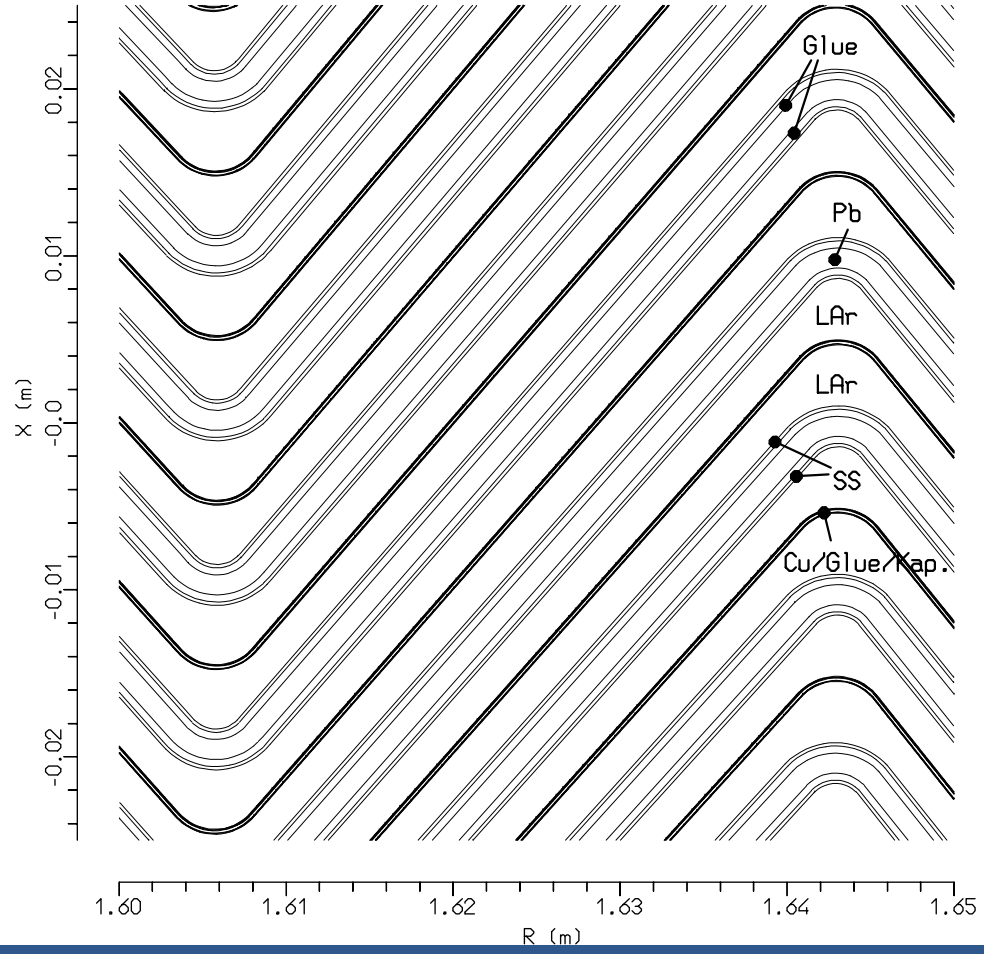

Sampling term :

e at $\eta = 0.28$

MC at 10 and 100 GeV

$$\text{Exp. :} \frac{\sigma}{E} = \frac{9.8 \pm 0.4\%}{\sqrt{(E)}}$$

$$\text{FLUKA :} \frac{\sigma}{E} = \frac{9.2 \pm 0.3\%}{\sqrt{(E)}}$$

Phi modulation of the response

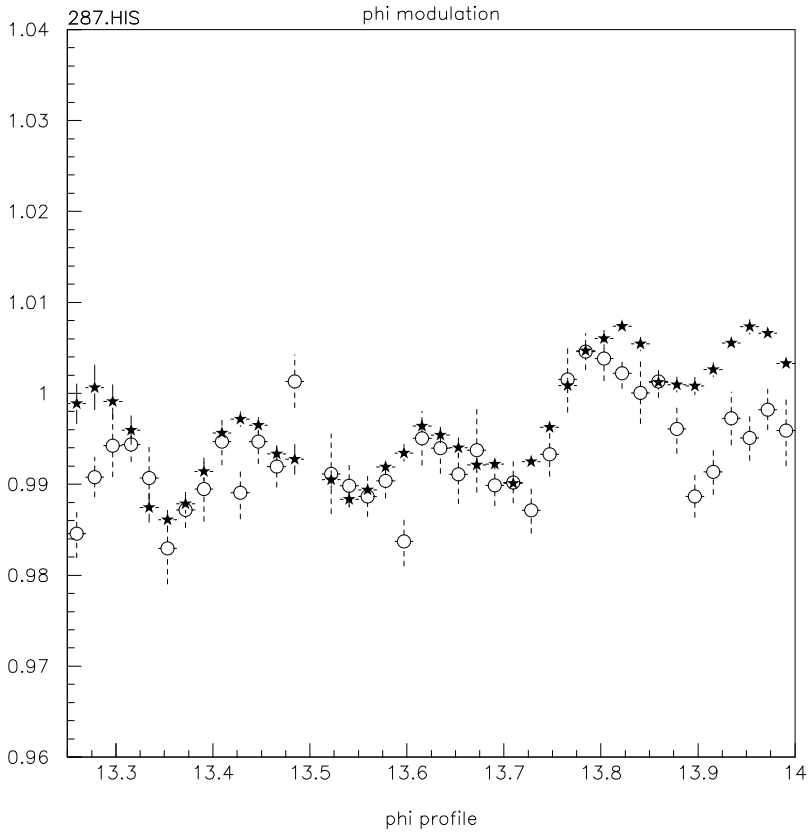

Longitudinal Development:

e at $\eta = 0.28$

Energy in sampling 1 / total

E	E1/E		r.m.s.	
GeV	Data	Fluka	Data	Fluka
100	0.68	0.69		
287	0.61	0.58	.091	.094

300 GeV μ in ATLAS combined calo

Calibration in electron scale
electronic noise added

E.M. Calorimeter

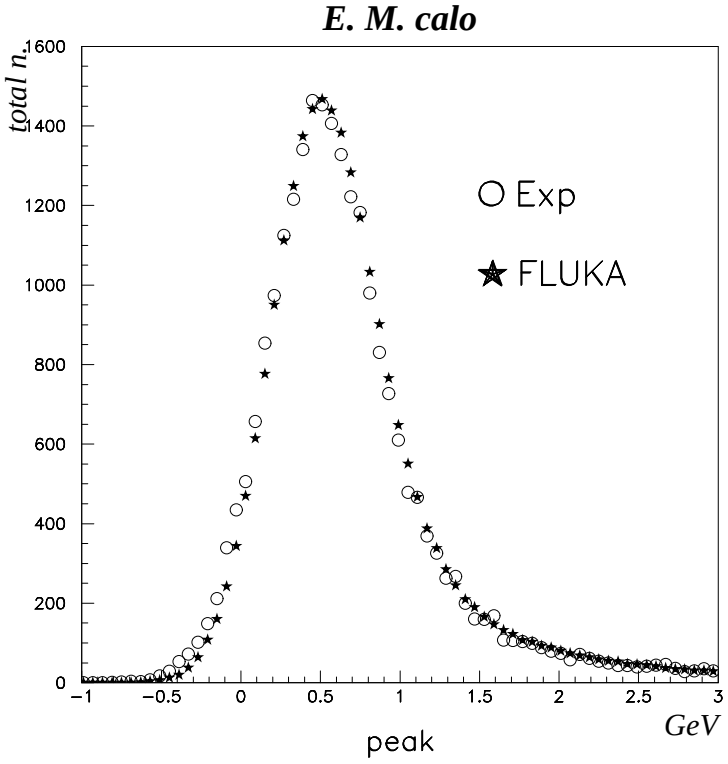

Tile Calorimeter

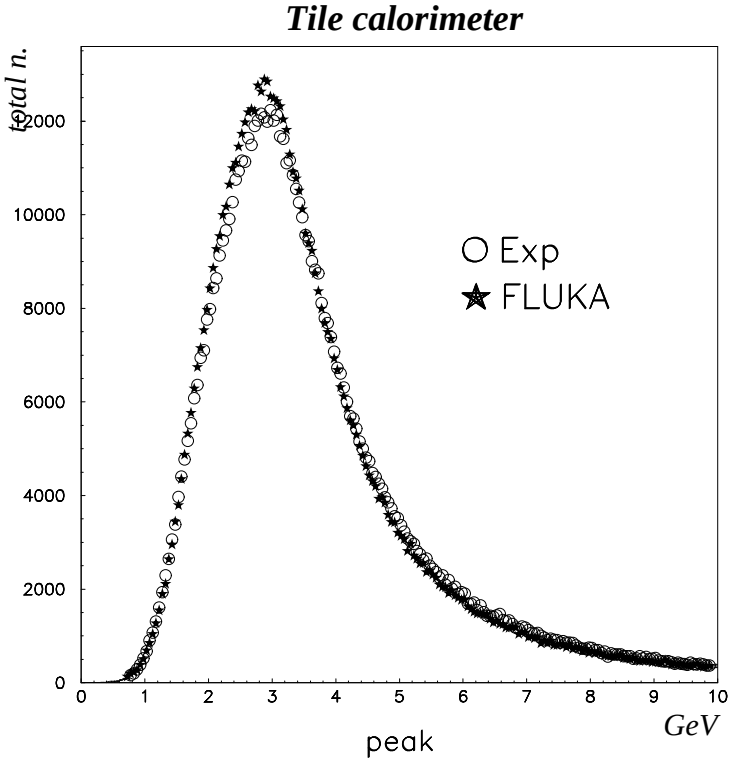

Comparison with PION data

Cut on mip in presampler Cut on beam position (beam chambers)

FLUKA: Calibration in electron scale

FLUKA: Scintillator quenching included, Noise added

FLUKA: Proton contamination taken into account

Energy reconstructed using the "benchmark" technique:

$$E_0 = E_{em} + a \cdot Q_{had} + b \cdot \sqrt{|E_{em_3} \cdot a \cdot Q_{had_1}|} + c \cdot E_{em}^2 \qquad (1)$$

All parameters fixed to minimize $\frac{\sigma}{E_0}$ *at 300 GeV*

Comparison with PION data

1994 Data: **Experimental electron scale calibration available**

	a (GeV/pC)	b	c (GeV^{-1})
FLUKA	0.172(2)	0.38(2)	-0.00038(10)
EXP	0.172	0.44	-0.00038

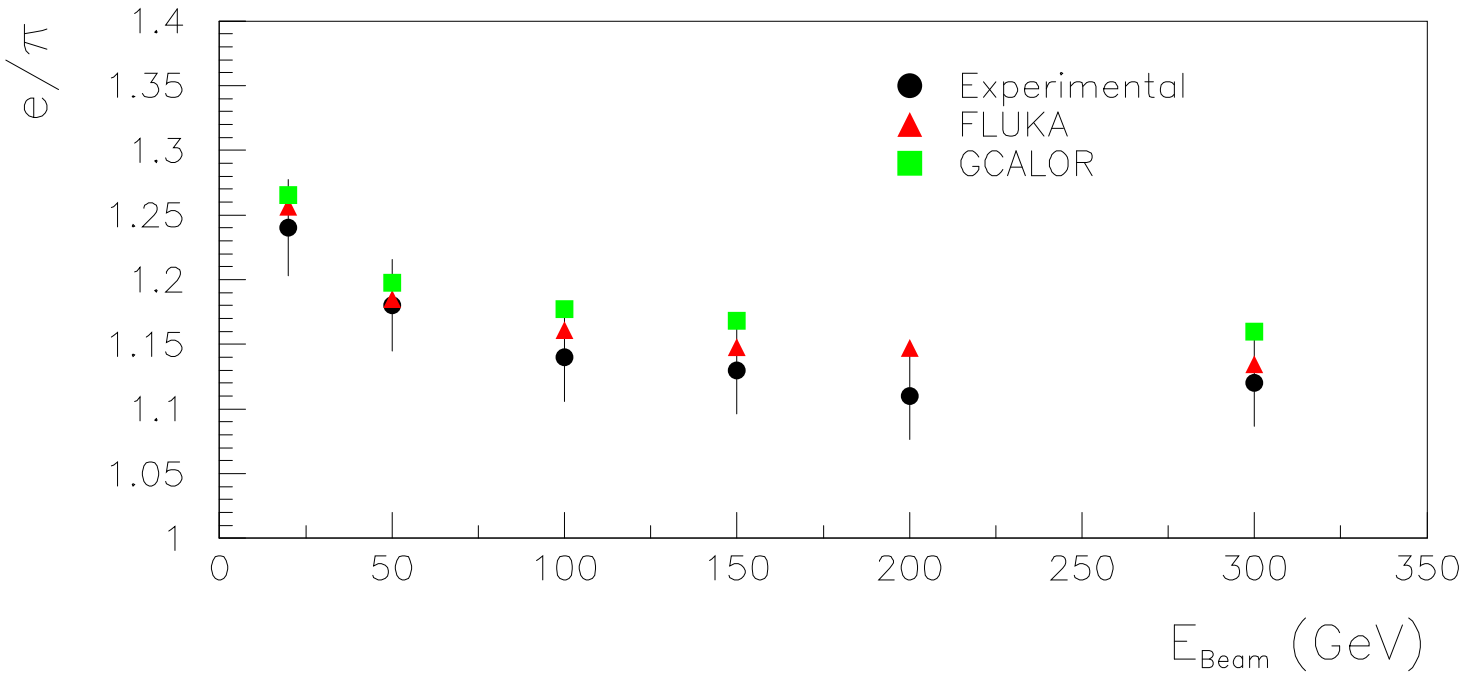

Comparison with PION data

1994 Data

Longitudinal shower development

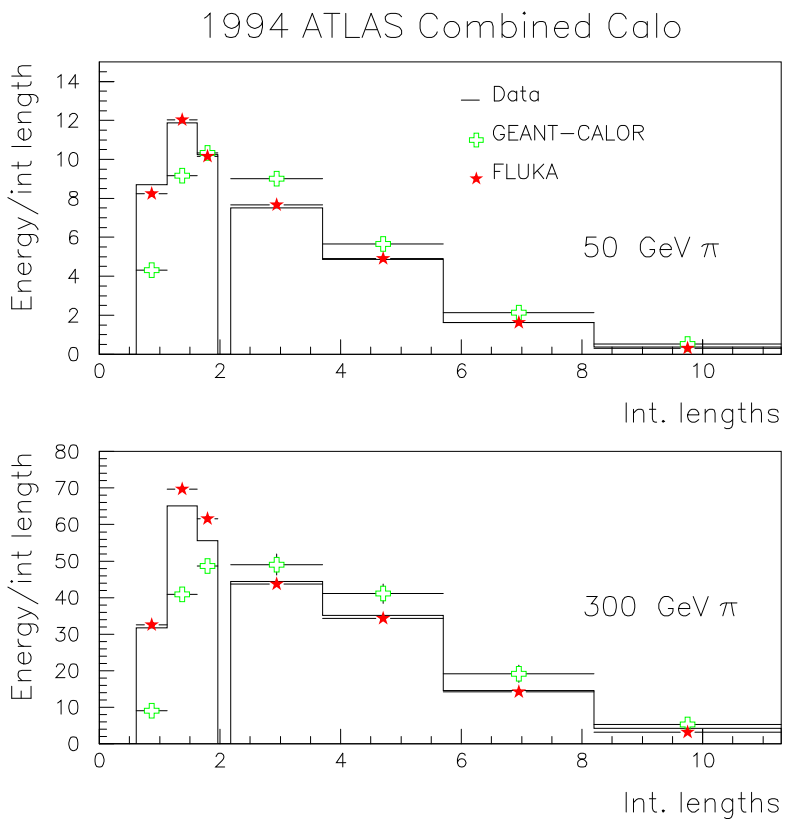

Energy spectrum in E.M. calo

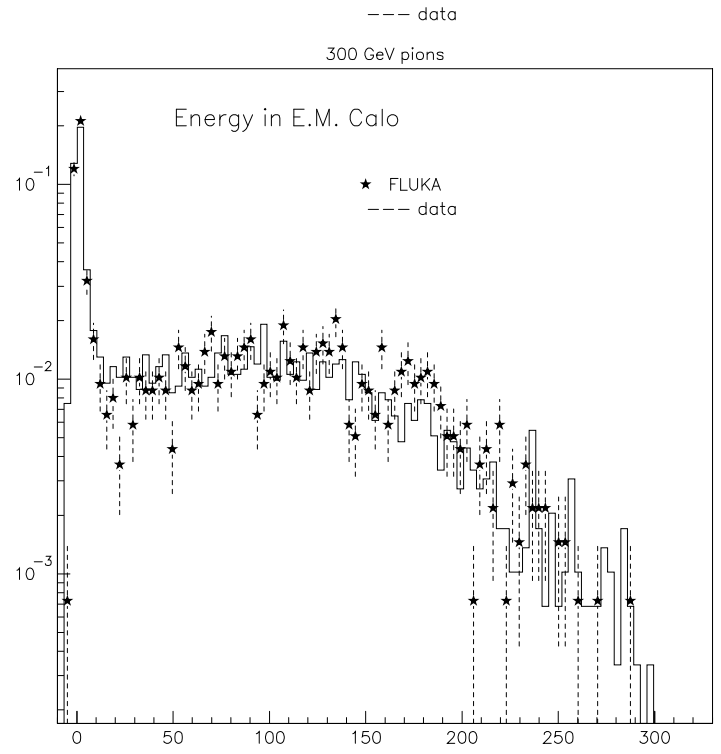

Comparison with pion data

Energy Resolution

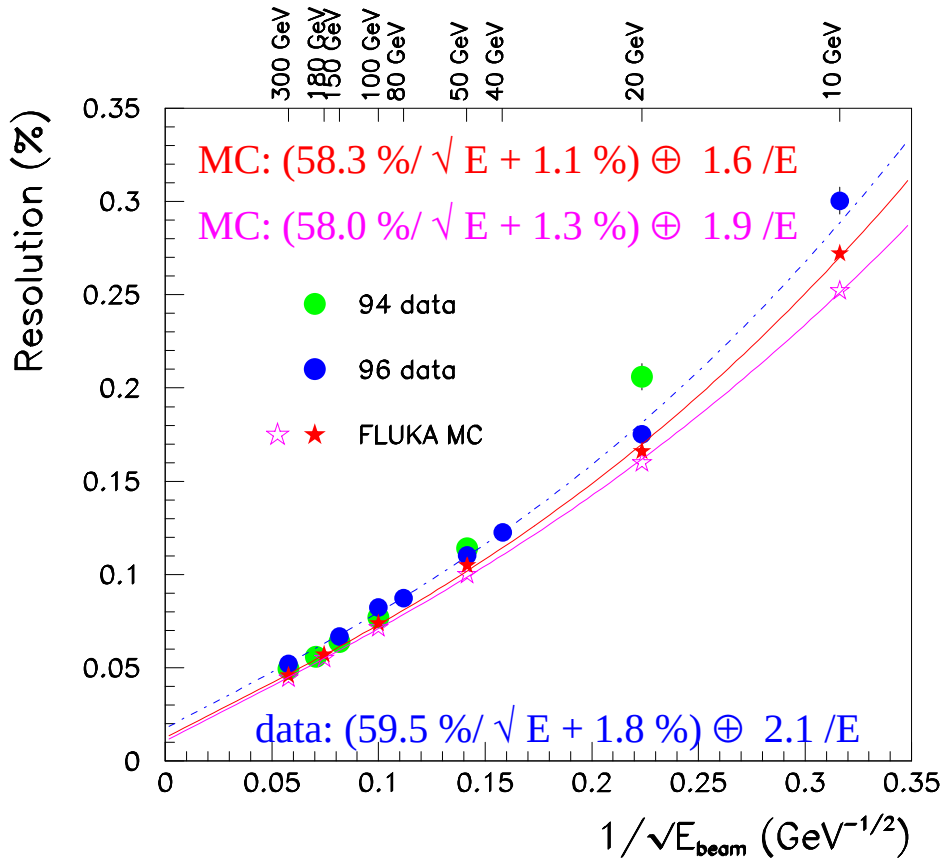

1996 Data :

Less electronic noise

Better presampler

No electron calibration

Comparison with pion data

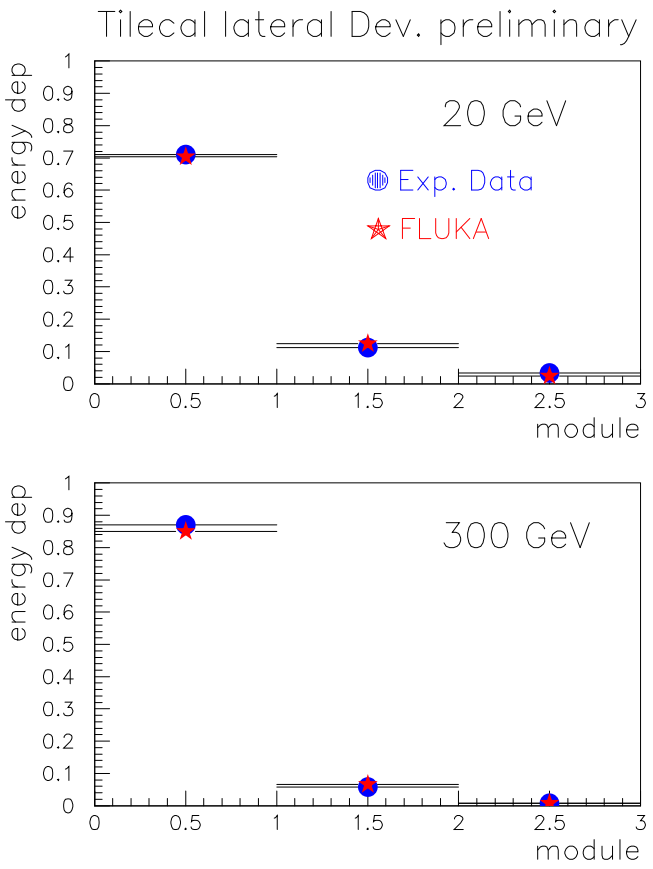

Linearity

1996 Combined Calo Test Beam

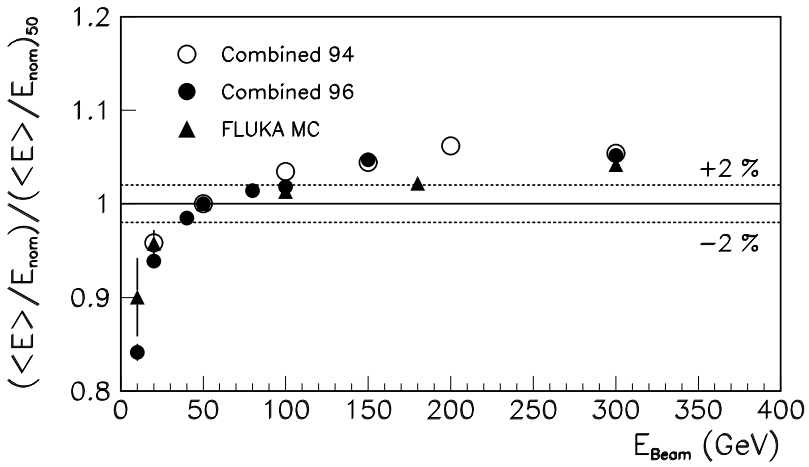

Effect of upstream materials presampler

Interactions in dead materials upstream → degradation of the beam

Cut on mip signal in presampler → cut degraded events

Exp. Problems: signal/noise, clustering

M.C. Problems: ..know all materials.., reproduce instrumental effects

M.C. need: reproduce correlations among all shower quantities

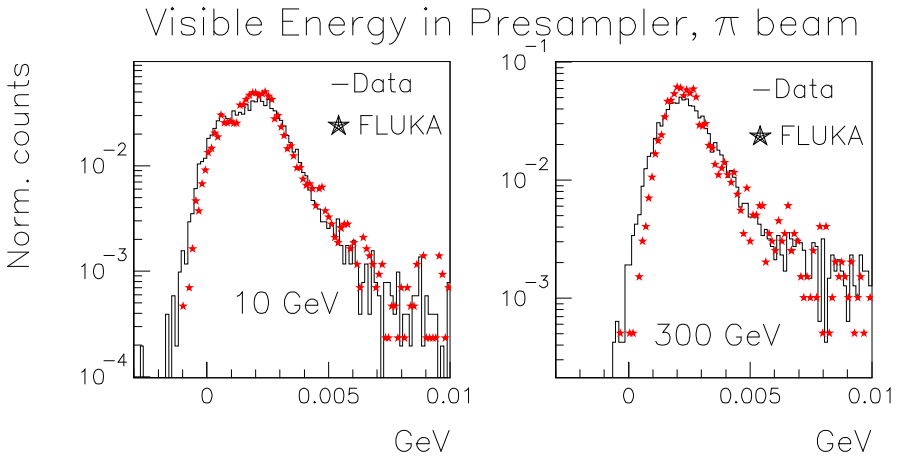

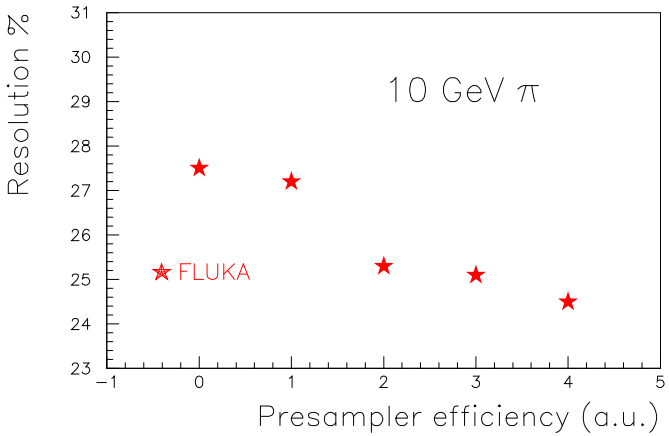

The effect of energy non-conservations

Include in each FLUKA interaction an energy non-conservation similar to the one observed in the old GEANT3-GHEISHA package as a function of projectile/energy

Simulation: Positive Pions in the ATLAS 1996 Combined Calo set-up

E(GeV)	Per Interaction		Per Event		σ/E	
	E_{miss}	rms	E_{miss}	rms	FLUKA	FLUKA+E_{miss}
10	0.094	0.25	2.1	0.93	24%	35%
100	0.070	0.28	12.7	5.3	7.2%	11.4%

$\Downarrow$

To enforce energy and momentum conservation at each step is as important as having sound physiccal models!!

The effect of quenching

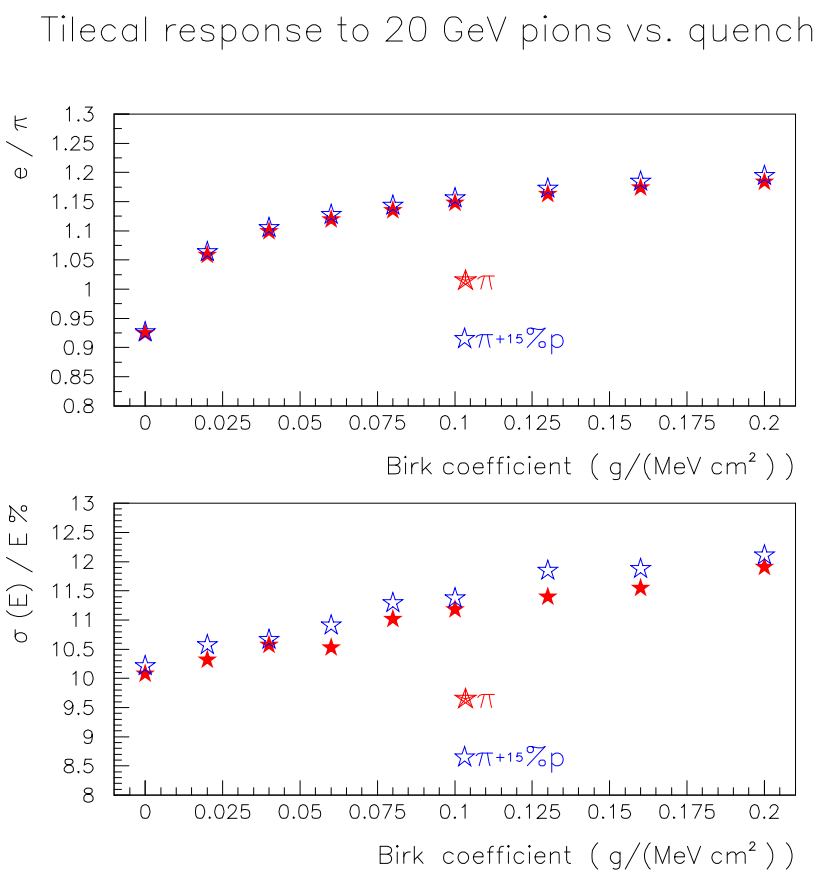

20 GeV/c π + 20 GeV/c protons

Tile calorimeter prototype

Fe-scintillator

"Naive" FLUKA simulations (no ph.stat., no noise, etc)

Conclusions

- Hadron interaction modelling is enough advanced to provide reliable estimates of particle production and propagation under most circumstances
- Most of the basic features of hadronic calorimetry can be understood in terms of specific aspects of hadron nuclear interactions
- All aspects related to energy conservation and binding energy losses are critical and deserve a proper treatment
- Slow neutrons are "by construction" a precise index of the amount of energy going into binding. A proper sampling of their signal, via nuclear γ's detection or oversampling of their recoils (hydrogen) is critical in order to reduce the intrinsic resolution
- The intrinsic resolution of hadronic showers is an ill-defined concept. Together with e/h it can vary wildly depending on the acceptance time window and quenching properties, for the same bulk characteristics
- Reasonable predictions for real life calorimeters can be obtained provided reliable models are used and with a deep understanding of all instrumental effects

Other applications: neutrino interactions

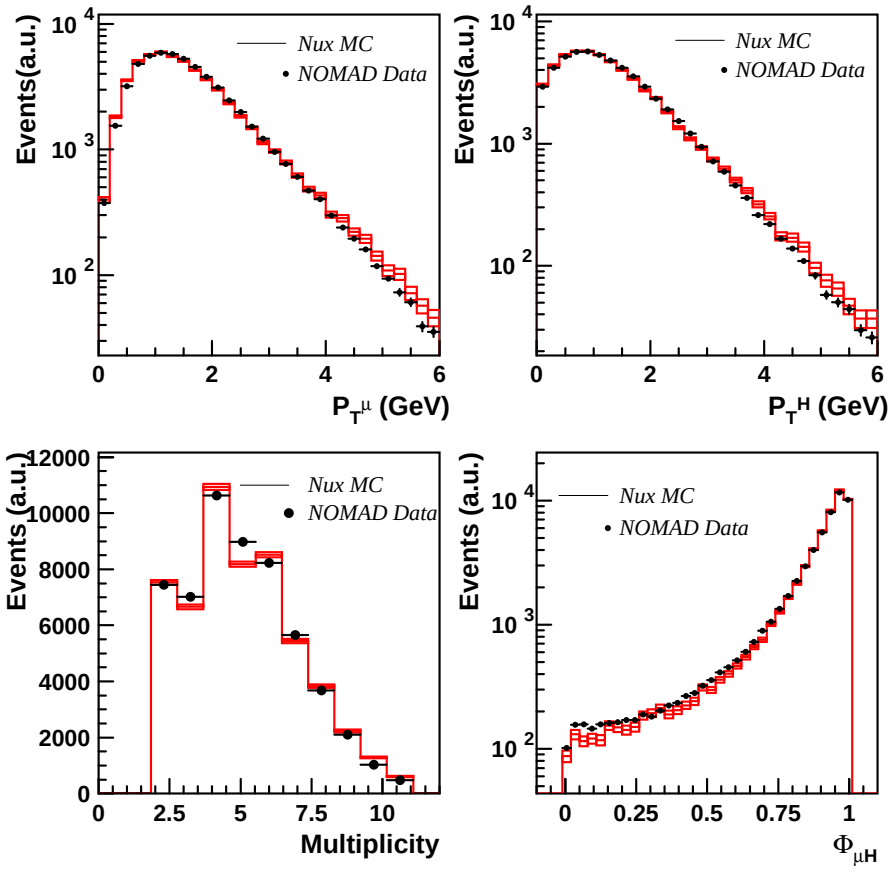

Comparison of various experimental observables for neutrino interactions as obtained with the NUX-FLUKA (A.Ferrari, A.Rubbia, P.R.Sala) neutrino event generator with NOMAD data (full simulation with NUX-FLUKA→ GNOMAD)

Other applications: neutrino interactions II

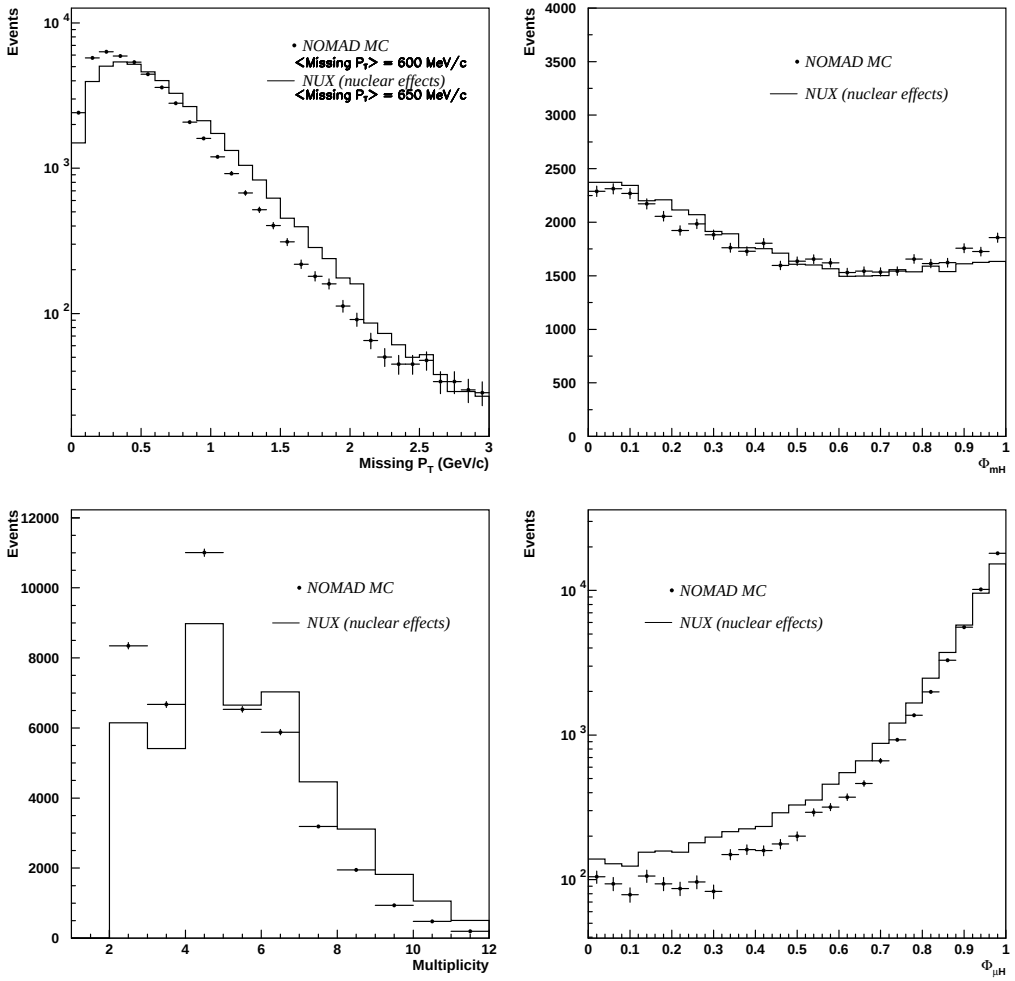

Infinite calorimeters: neutrinos

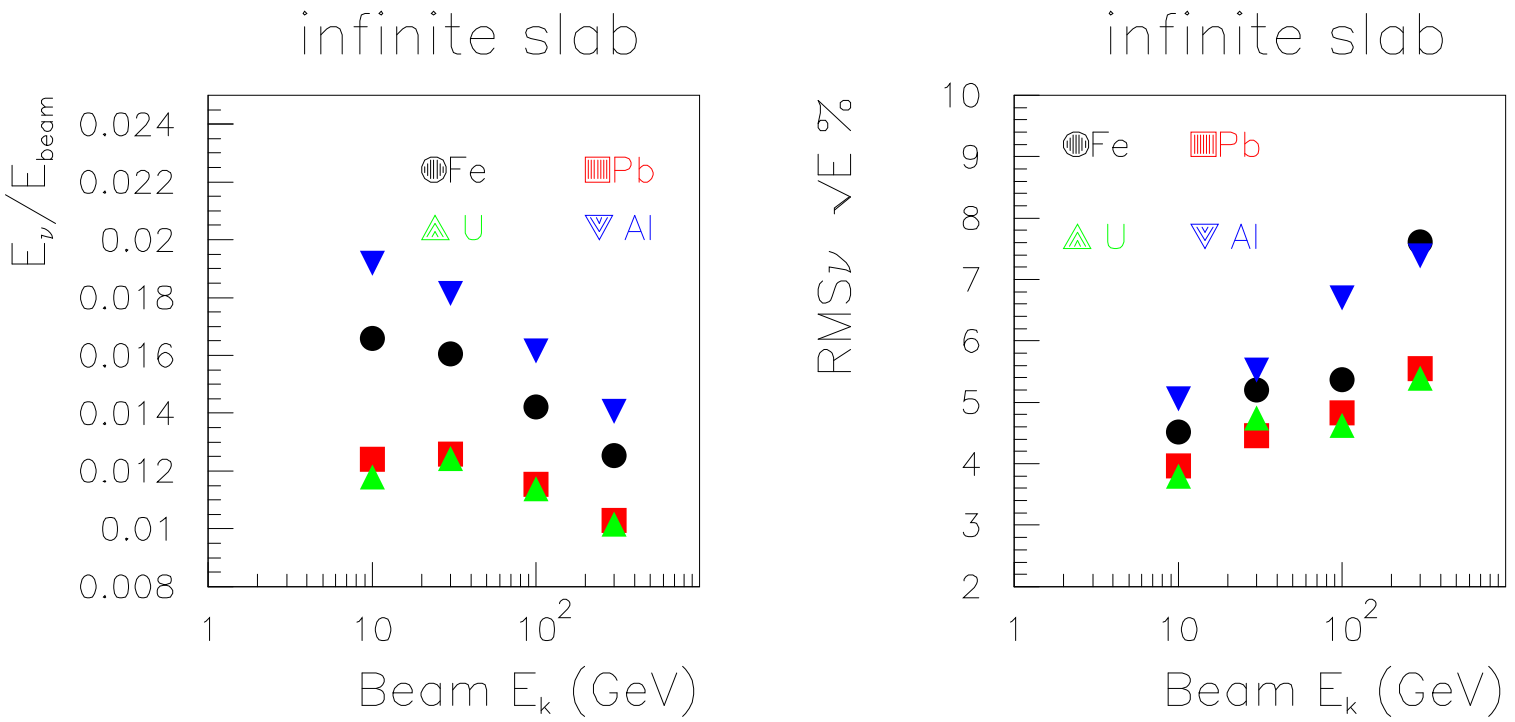

Average neutrino energy fraction (left) and fractional rms (right) as a function of energy for a proton beam.

Dual Parton Model: introduction

Dual Parton Model (DPM): originally developed in Orsay in 1979. Together with similar models, i.e. the Quark Gluon String Model (QGSM) developed independently in Russia, it provides a framework for the description of the soft component of high energy hadronic interactions

Recently these models have been extended to include in a coherent approach the hard component as predicted by perturbative QCD.

DPM, QGSM and similar approaches are the theoretical framework adopted by the vast majority of models/codes describing hadronic interactions at accelerator and cosmic ray energies in the 80's and in the 90's

DPM is the framework of choice for the model developed for FLUKA in order to describe hadron-nucleon interaction from several GeV onwards

DPM: generalities

- Problem: the features of "soft" interactions (low-p_T interactions) cannot be derived from the QCD Lagrangian, because the large value taken by the running coupling constant prevents the use of perturbation theory.
- QCD: gluons are coloured $\rightarrow$ strongly self-interacting. Suppose quarks are held together by color lines of force, the gluon-gluon interaction will pull them together into the form of a tube or a string. Since quarks are confined, the energy required to "stretch" such a string is increasingly large until it suffices to materialize a quark-antiquark couple from the vacuum and the string breaks into two shorter ones, with still quarks at both ends.
- Hence because of quark confinement, theories based on interacting strings are powerful tools in understanding QCD at the soft hadronic scale, that is in the non-perturbative regime.
- An interacting string theory naturally leads to a topological expansion. At high energies, such an expansion was developed already before the establishment of QCD, $\rightarrow$ the Reggeon-Pomeron calculus in the framework of perturbative Reggeon Field Theory.

The Dual Parton Model is built introducing partonic ideas into a topological expansion which explicitly incorporates the constraints of duality and unitarity, typical of Regge's theory.

DPM: generalities cont.

DPM: hadron considered as open strings with quarks, antiquarks or diquarks sitting at the ends

- mesons (colorless combination of a quark and an antiquark $q\bar{q}$): strings with their valence quark and antiquark at the ends.
- (Anti)baryons (colorless combinations of three (anti)quarks, qqq): open strings with a (anti)quark and a (anti)diquark at the ends.
- At sufficiently high energies the leading term corresponds to a Pomeron (IP) exchange (a closed string exchange), which has a cylinder topology.
- When an unitarity cut is applied to the cylindrical Pomeron two hadronic chains are left as the sources of particle production.
- While the partons out of which chains are stretched carry a net color, the chains themselves are built in such a way to carry no net color, or to be more exact to constitute color singlets like all naturally occuring hadrons.

In practice, as a consequence of color exchange in the interaction, each colliding hadron splits into two colored system, one carrying color charge c and the other $\bar{c}$. These two systems carry together the whole momentum of the hadron. The system with color charge c ($\bar{c}$) of one hadron combines with the system of complementary color of the other hadron, in such a way to form two color neutral chains. These chains appear as two back-to-back jets in their own centre-of-mass systems.

DPM: chain building

The exact way of building up these chains depends on the nature of the projectile-target combination (baryon-baryon, meson-baryon, antibaryon-baryon, meson-meson):

Let be $q_p^v(\bar{q}_p^v)$ the valence (anti)quarks of the projectile, and with q_t^v those of the target, and assume that the (anti)quarks sitting at one end of the baryon strings carry momentum fraction x_p^v and x_t^v respectively

- baryon-baryon scattering chains: $q_t^v - q_p^v q_p^v$ and $q_p^v - q_t^v q_t^v$
- meson-baryon scattering chains: $q_t^v - \bar{q}_p^v$ and $q_p^v - q_t^v q_t^v$
- antibaryon-baryon scattering chains: $q_t^v - \bar{q}_p^v$ and $\bar{q}_p^v \bar{q}_p^v - q_t^v q_t^v$

DPM: chain examples

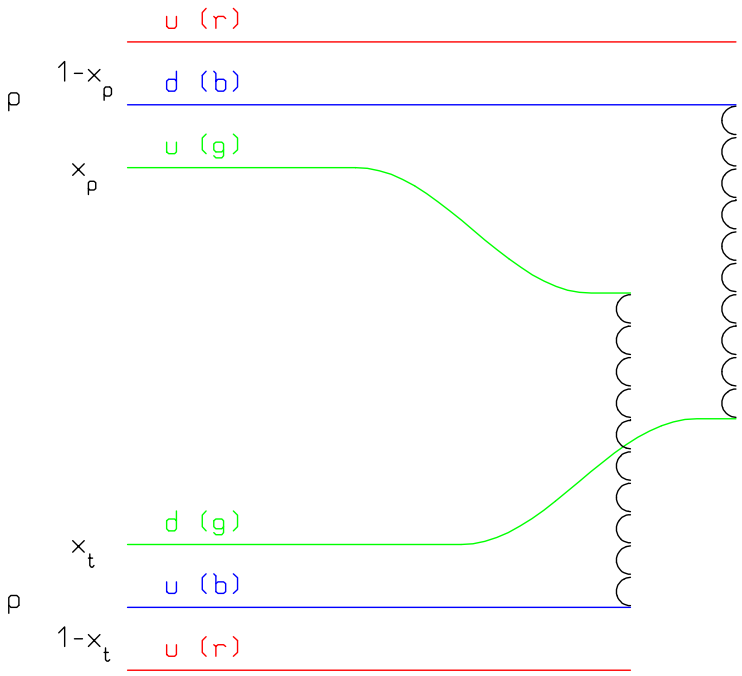

Leading two-chain diagram in DPM for $p-p$ scattering. The color (red, blue, and green) and quark combination shown in the figure is just one of the allowed possibilities

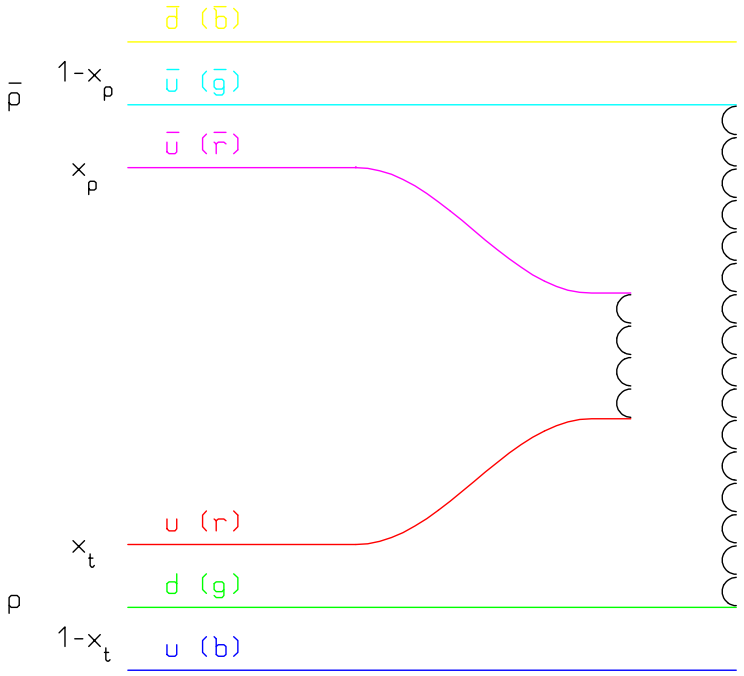

Leading two-chain diagram in DPM for $\bar{p}-p$ scattering. The color (red, blue, and green) and quark combination shown in the figure is just one of the allowed possibilities

DPM: chain examples II

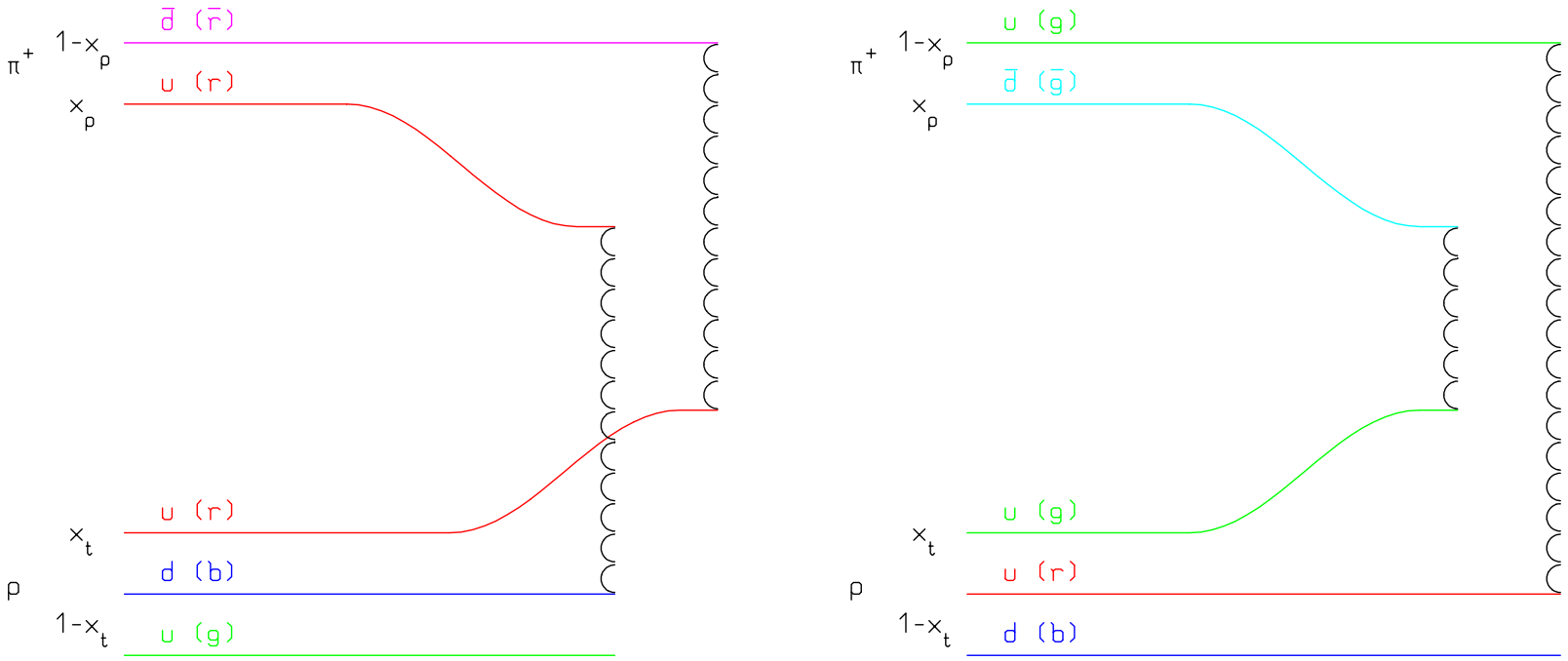

Leading two-chain diagrams in DPM for $\pi^+ - p$ scattering. The color (red, blue, and green) and quark combination shown in each figure is just one of the allowed possibilities

DPM: chain energies and momenta

The energy and momentum in the centre-of-mass system of the collision, as well as the invariant mass squared of the two chains, are given by:

$$
\begin{aligned}
E^*_{ch1} &\approx \frac{\sqrt{s}}{2}(1 - x^v_p + x^v_t) \\
E^*_{ch2} &\approx \frac{\sqrt{s}}{2}(1 - x^v_t + x^v_p) \\
p^*_{ch1} &\approx \frac{\sqrt{s}}{2}(1 - x^v_p - x^v_t) = -p^*_{ch2} \\
s_{ch1} &\approx s(1 - x^v_p)x^v_t \\
s_{ch2} &\approx s(1 - x^v_t)x^v_p
\end{aligned}
$$

DPM: multiple soft chains

The single Pomeron exchange diagram is the dominant contribution, however higher order contributions with multi-Pomeron exchanges become important at energies in excess of 1 TeV in the laboratory

They correspond to more complicated topologies, and DPM provides a way for evaluating the weight of each, keeping into account the unitarity constraint

When cut, every extra Pomeron exchanged gives rise to two extra chains which are built using two $q\bar{q}$ couples excited from the projectile and target hadron sea respectively.

The inclusion of these higher order diagrams is usually referred to as *multiple soft collisions*.

DPM: momentum distributions

The exact form of the momentum distribution for the x variables of valence and sea quarks, $P(x_1, .., x_n)$, is unknown.

However, general considerations based on Regge arguments allow to predict the asymptotic behaviour whenever each of its arguments goes to zero.
The behaviour turns out to be singular in all cases, but for the diquarks.

A reasonable assumption is therefore to approximate the true unknown distribution function with the product of all these asymptotic behaviours, treating all the rest as a normalization constant

DPM: momentum distributions II

Under this approximation, indicating with $x_{q\ i}^{sea}$, and $x_{\bar{q}\ i}^{sea}$, the energy/momentum fractions carried by the sea quarks and with X_i^{sea} the sum of $x_{q\ i}^{sea}$ and $x_{\bar{q}\ i}^{sea}$, the total momentum distribution function for a(n) (anti)baryon in the case of $n_{I\!P}$-cut Pomerons can be written as:

$$\begin{aligned} P(\bar{x})\mathrm{d}\bar{x} &\approx C_b\ x_q^{-\frac{1}{2}} x_{qq}^{\frac{3}{2}} \prod_i^{n_{I\!P}-1} (X_i^{sea})^{-1} (x_{q\ i}^{sea})^{-\frac{1}{2}} (x_{\bar{q}\ i}^{sea})^{-\frac{1}{2}} \\ &\cdot \delta(1 - x_q - x_{qq} - \sum_i^{n_{I\!P}-1} X_i^{sea})\ \mathrm{d}\bar{x} \qquad (2) \\ \bar{x} &\equiv x_q \cdot x_{qq} \prod_i^{n_{I\!P}-1} \left(x_{\bar{q}\ i}^{sea} \cdot x_{q\ i}^{sea}\right) \end{aligned}$$

where C_b is a normalization factor. The momentum distribution function for a meson reads:

$$\begin{aligned} P(\bar{x})\mathrm{d}\bar{x} &\approx C_m\ x_q^{-\frac{1}{2}} x_{\bar{q}}^{-\frac{1}{2}} \prod_i^{n_{I\!P}-1} (X_i^{sea})^{-1} (x_{q\ i}^{sea})^{-\frac{1}{2}} (x_{\bar{q}\ i}^{sea})^{-\frac{1}{2}} \\ &\cdot \delta(1 - x_q - x_{\bar{q}} - \sum_i^{n_{I\!P}-1} X_i^{sea})\ \mathrm{d}\bar{x} \\ \bar{x} &\equiv x_q \cdot x_{\bar{q}} \prod_i^{n_{I\!P}-1} \left(x_{\bar{q}\ i}^{sea} \cdot x_{q\ i}^{sea}\right) \end{aligned}$$

Chain hadronization

The latter ingredient is a *hadronization model*, which must take care of transforming each chain into a sequence of physical hadrons, stable ones or resonances

The basic assumption is that of *chain universality*, which assumes that once the chain ends and the invariant mass of the chain are given, the hadronization properties are the same regardless of the physical process which originated the chain

Therefore the knowledge coming from hard processes and e^+e^- collisions about hadronization can be used to fulfill this task. There are many more or less phenomenological models which have been developed to describe hadronization. In principle hadronization properties too can be derived from Regge formalism

DPM: summary

Summarizing, DPM provides recipes for performing the following tasks:

- determining the number of cut Pomerons, and therefore the number of chains contributing to the reaction
- forming the chains using the valence and possibly sea quarks of the two colliding hadrons
- determining the energy and momentum carried by each chain, according to the momentum distribution functions of the two colliding hadrons
- hadronizing each chain producing the final hadrons, stable ones or resonances

The last step is not exactly a part of DPM, but rather DPM is factorized in such a way that it can be accomplished using whichever hadronization scheme. In principle there is little or no freedom in each individual step, therefore strenghtening the predictive power of the model
Actually, in the energy range of interest for experiments, threshold effects are still very important. While DPM is assumed to be valid in the asymptotic regime, and treats massless partons at energies large enough to neglect hadron masses,most practical implementations deal with chains with invariant masses so small that only few particles can be produced out of the chain itself

It is possible to extend DPM to hadron-nucleus collisions making use of the Glauber-Gribov approach. Furthermore DPM provides a theoretical framework for describing hadron diffractive scattering both in hadron-hadron and hadron-nucleus collisions.